Identifying Changes in Myocardial Microstructure via a Novel Sonographic Imaging Algorithm

Citation

Hiremath, Pranoti. 2015. Identifying Changes in Myocardial Microstructure via a Novel Sonographic Imaging Algorithm. Doctoral dissertation, Harvard Medical School.

Permanent link

http://nrs.harvard.edu/urn-3:HUL.InstRepos:15821586

Terms of Use

Share Your Story

Abstract

Echocardiography is a widely accessible imaging modality that is conventionally used for non-invasive characterization of cardiac structure and function. Analyses of cardiac tissue may be performed through ultrasound assessments of grayscale signal intensity within pre-selected regions of interest. Prior techniques have relied predominantly on the mean backscatter signal intensity; however, mean values have demonstrated low specificity and sensitivity, and may be susceptible to variability from low frame rates and time delays. We describe an ultrasound-based imaging algorithm that extends from previous methods, can be applied to a single image frame using open-access image analysis software, and accounts for the full distribution of signal intensity values within a region of interest. Specifically, our algorithm is used to assess left ventricular myocardial microstructure based on analysis of the reflection intensity at the myocardial-pericardial interface on B-mode echocardiographic images. The algorithm produces a measurement value, termed the signal intensity coefficient (SIC), which can serve as an enhanced surrogate measure of myocardial microstructure.

The transition from healthy myocardium to heart disease is characterized by a series of poorly understood changes in myocardial tissue microstructure. Incremental alterations in the orientation and deformation of myocardial fibers can be assessed using advanced ultrasonic image analysis. Therefore, we assessed the ability to evaluate performance of the SIC in the setting of two different heart disease phenotypes.

First, we evaluated the extent to which the SIC can quantify differences between normal myocardium and hypertensive heart disease in humans as well as in a mouse model of afterload resistance. We compared the SIC to tissue histology in mice and conventional echocardiographic measures in both mice and humans. In mice exposed to varying degrees of afterload stress,

1

algorithm measurements (P=0.026) compared with left ventricular (LV) mass (P=0.053) more clearly differentiated between animal groups that underwent fixed aortic banding, temporary aortic banding, or sham procedure, on echocardiography at 7 weeks after surgery. The algorithm significantly differentiated between ambulatory adults with uncomplicated essential hypertension (N=30) and healthy controls (N=28) after adjusting for age and sex (P=0.025). There was a trend in higher LV relative wall thickness in hypertensive individuals compared to controls (P=0.08), but no difference between groups in left ventricular mass (P=0.98) or absolute LV wall thickness (P=0.37).

Second, we evaluated performance of the SIC in the setting of hypertrophic cardiomyopathy (HCM), a genetically transmitted disease characterized by heterogeneous tissue changes including fibrosis. Thus, we also evaluated the ability of the SIC to reveal changes in myocardial tissue in sarcomere mutation carriers with overt and subclinical HCM compared to healthy controls. We compared the SIC with conventional echocardiographic measures of structure and function, serum biomarkers, and an MRI-based assessment of extracellular volume (ECV), which is considered a surrogate measure of myocardial fibrosis.

In the HCM study sample, the SIC was significantly correlated with echocardiographic LV wall thickness (R=0.61, P<0.001), echocardiographic global E' velocity, (R=-0.84, P<0.001), and MRI-based ECV (R=0.85, P<0.001). Conventional echocardiographic measures of LV mass and wall thickness, and serum biomarkers, were significantly different when comparing overt (N=10) with subclinical HCM (N=10), but not when comparing subclinical HCM with healthy controls (N=10). By contrast, global E' velocity, SIC, and ECV significantly distinguished between all groups, including individuals with subclinical HCM versus healthy controls (P<0.01).

Based on sonographic signal intensity analysis, a novel imaging algorithm provides an accessible, non-invasive measure that appears to differentiate normal LV microstructure from myocardium exposed to chronic afterload stress, as demonstrated in mice and humans. The algorithm may also serve as a marker of subclinical HCM in sarcomere mutation carriers, revealing changes in cardiac tissue prior to the development of overt HCM disease.

In summary, the SIC algorithm appears to be a particularly sensitive measure of the myocardial changes that occur early in the course of disease progression in both hypertensive heart disease and HCM. Thus, the SIC may serve as a useful tool for characterizing tissue-level changes involved in cardiac remodeling during pathogenesis as well as response to treatments of HCM and hypertensive heart disease.

Table of Contents

Glossary of Abbreviations

BP	Blood pressure
CMR	Cardiac magnetic resonance imaging
DBP	Diastolic blood pressure
DICOM	Digital imaging and communication in medicine, an imaging file format
ECV	Extracellular volume, an MRI-based assessment of fibrosis
G+/LVH+	Overt HCM: genotype positive, left ventricular hypertrophy positive
G+/LVH-	Subclinical HCM: genotype positive, LV hypertrophy negative
G-/LVH-	Healthy controls: genotype negative, left ventricular hypertrophy negative
HCM	Hypertrophic cardiomyopathy
HF	Heart failure
LGE	Late gadolinium enhancement
LV	Left ventricle
LVDD	Left ventricular end-diastolic diameter
LVEF	Left ventricular ejection fraction
LVH	Left ventricular hypertrophy
LVFS	Left ventricular fractional shortening
LVSD	Left ventricular end-systolic diameter
LVWT	Left ventricular wall thickness
MAP	Mean arterial pressure
MRI	Magnetic resonance imaging
NT-proBNP	N-terminal prohormone of brain natriuretic peptide
PICP	Procollagen type I carboxy-terminal peptide
ROI	Region of interest
RWT	Relative wall thickness
SBP	Systolic blood pressure
SIC	Signal intensity coefficient
TnI	Cardiac troponin I

Introduction

Cardiac Remodeling: Microstructure to Macrostructure

Cardiac remodeling describes the molecular, cellular, and interstitial changes that lead to altered size, shape, and function of the heart.[1] In multiple forms of myocardial disease, molecular pathways progress to macrostructural cardiac changes in response to diverse influences including volume overload, pressure overload, genetic mutations, and neurohormonal processes.[1-5] Ventricular changes secondary to cardiac remodeling may ultimately result in clinical symptoms of heart failure (HF) and arrhythmias secondary to electro-mechanical dysfunction.[1, 2]

Elevated afterload stress and genetic mutations are among the etiologies that have been implicated in adverse cardiac remodeling. Hypertension, which creates elevated afterload stress upon the heart, is the most common risk factor for changes in LV structure and function as seen in HF.[6] However, the pathogenesis remains unclear.[4] The classic paradigm of cardiac remodeling in hypertension involves LV wall thickening in response to increased high wall stress from elevated blood pressure. This initial remodeling is followed by a "transition to failure" characterized by eventual LV dilation and a measurable decrease in LV ejection fraction.[6, 7] Although cardiac remodeling caused by elevated afterload stress can occur independently of heritable traits, genetic mutations may also drive cardiac remodeling, leading to subsequent changes in LV structure and function. Dilated cardiomyopathy may result from 25 chromosome loci, and hypertrophic cardiomyopathy (HCM) may result from mutations in 11 genes that encode sarcomere proteins.[2] Although mutations in different HCM genes have been associated with distinct clinical manifestations, the time course and extent of remodeling varies even for individuals of the same genotype.[8] Genetic heterogeneity in cardiac remodeling, together with

the heterogeneity of macrostructural phenotypes following cardiac remodeling, supports the presence of multiple pathways contributing to myocardial disease.

A growing body of evidence suggests that changes at the tissue level, or "microstructure," may occur at pre-clinical stages of disease and may precede overt clinical disease caused by macrostructural cardiac remodeling.[6, 9] Recent studies have demonstrated that "subclinical" HCM sarcomere mutation carriers may develop tissue changes prior to overt LV hypertrophy.[8, 10-13] Investigators have hypothesized that genetic mutations involved in HCM cause dysregulation of energy handling and calcium homeostasis within the myocardium, resulting in myocyte hypertrophy, disarray, and fibrosis.[11, 13-15] Similarly, chronic exposure to afterload stress has been shown to create heterogeneous changes in the cardiac microstructure prior to clinical stages of HF.[1, 16, 17] Observed microstructural changes include myocyte lengthening, myocyte widening, collagen accumulation, fibrosis, and remodeling of the extracellular matrix.[1, 5]

Many pre-clinical cardiac remodeling changes may be reversible, and may occur at a time when medical interventions can alter the course of disease. Existing medications such as ACE inhibitors and beta blockers oppose adverse remodeling, and additional therapies are under development to target fibroblasts and emerging molecular pathways of disease.[18, 19] Interventional therapies, including valvular repair and implantable devices, may also reverse advanced stages of cardiac remodeling.[1, 20] However, medications and interventional therapies may provide only partial reversal of cardiac remodeling, and may not sufficiently reverse adverse effects of disease. For example, a study of patients with mitral regurgitation demonstrated that abnormal preoperative atrial and ventricular dimensions were predictive of decreased reverse remodeling following mitral valve repair.[3] In a trial of valsartan in patients with LV dysfunction, although valsartan demonstrated the greatest anti-remodeling effect and clinical benefit in

individuals with higher baseline severity of remodeling, these individuals were also at highest risk for a major cardiac event.[21] Evidence suggests that, despite the advent of therapies that reverse cardiac remodeling, the majority of treatments are most effective when applied to early stages of cardiac remodeling, prior to the development of more advanced structural alterations. Therefore, a key goal is to develop tools to identify at-risk individuals most likely to benefit from early intervention. Conventional methods for assessment of cardiac remodeling include conventional cardiac imaging, histology, and serum biomarkers. Serum biomarkers (including N-terminal prohormone of brain natriuretic peptide, procollagen type I carboxy-terminal peptide, and cardiac troponin I) have demonstrated limited specificity in describing disease progression.[22-24] Tissue-level characterization of the myocardial microstructure could be as sensitive or even more sensitive than detectable biomarker elevations and changes in left ventricular gross morphology,[16, 25, 26] because microstructural changes could reflect cellular and extracellular alterations occurring very early in response to cardiac stress (**Figure 1**). Histologic studies have been used to evaluate increases in myocyte size, accumulation of interstitial fibrosis, and extracellular matrix deposition in the myocardium as well as around the myocardial vasculature.[27, 28] Although histologic assessment is the gold standard for tissue analysis, it requires invasive procedures to obtain tissue, limiting its use in both clinical and experimental studies.

Non-invasive imaging provides the opportunity to investigate changes in left ventricular morphology in both experimental models and clinical studies. Conventional cardiac ultrasound (i.e. echocardiography) has long been used to identify the presence of LV hypertrophy, defined by macroscopic measures of LV mass. However, changes in LV function are known to occur in the setting of LV structure that appears normal by conventional echocardiography.[25-27] This discrepancy is due to the fact that conventional diagnostic techniques have limited sensitivity to

microstructural changes, which precede changes in gross morphology. The ability to non-invasively identify abnormalities in LV microstructure that accompany and even precede changes in LV function would facilitate efforts to better characterize the earliest changes that occur in cardiac remodeling, and would have potential to identify at-risk individuals most likely to benefit from early intervention.

Methods of Microstructural Imaging

Ultrasonic indices may be able to distinguish pathological tissue properties including myocardial disarray, size heterogeneity, increased myocyte density, and interstitial fibrosis.[29, 30] Investigators have hypothesized that these properties alter tissue impedances, thereby changing sonographic signal reflections, and altering echocardiographic grayscale images uniquely for each individual's myocardial characteristics.[29, 31-33] Upon isolating a specific region of interest within the image, and then assigning a grayscale intensity value to each pixel within the ROI,[34, 35] data may be represented as frequency histograms of grayscale values, also known as signal intensity distributions (**Figure 2**). Pathological changes within the myocardial microstructure may influence signal intensity distributions, forming specific analyzable trends that are unique to the scattering properties of the imaged LV wall. In turn, patterns within the signal intensity distributions may be used to understand disease-specific myocardial microstructural changes.

Microstructural imaging methods using MRI and ultrasound have previously been applied in numerous clinical settings. CMR-based measures of late gadolinium enhancement (LGE) and extracellular volume (ECV) provide a method for quantification of tissue-level changes including cardiac interstitial fibrosis.[8, 11, 14] Diffusional kurtosis imaging, also an MRI-based technique, has been used to characterize brain neoplasms[36] and neurological degenerative disease.[37] Sonographic techniques have been used to assess liver cirrhosis,[38, 39] fetal and uterine

tissue,[40, 41] and myocardial tissue alterations. Previously developed cardiac ultrasound image analysis techniques, such as integrated backscatter, have been used in clinical contexts (**Table 1**) including hypertension,[31] early myocardial infarction,[32] chronic coronary artery disease,[42] and hypothyroidism.[43, 44] However, previously established methods have been limited by low sensitivity and specificity, particularly in the setting of poorer quality images.[45] Integrated backscatter and cyclic variation techniques, for example, depend predominantly on mean signal values.[46-48] Limitations to prior ultrasound-based techniques include increased variability from random noise,[49] susceptibility to time delays arising from the application of complex algorithms,[50, 51] and limited correlation with the extent of myocardial fibrosis present.[45] Despite the limitations of previous methods, advanced echocardiographic microstructural methods could provide an ultrasound-based assessment of tissue changes in cardiac remodeling, and could complement and extend existing imaging techniques.

Purpose of Inquiry

We developed a modified ultrasound-based image analysis algorithm using distributions of sonographic signal intensity values, and assessed the ability of our algorithm to quantify LV wall microstructural alterations.[52] We hypothesized that cardiac remodeling changes that result in cellular and extracellular alterations of the LV myocardium can be quantified using sonographic signal intensity distributions. Unlike previous techniques, which have focused on mean backscatter values, our method was developed upon analyzing techniques to capture variation across distributions of grayscale intensity values. Analyses of the complete distribution of grayscale values provide more informative and robust assessments of signal changes compared to the use of a mean value alone.

Following initial algorithm development, we evaluated the ability of the algorithm to assess early cardiac remodeling in hypertensive heart disease[34] and in HCM. In the assessment of hypertensive heart disease, the algorithm was applied to a mouse model of chronic afterload stress and a human cohort with variable exposure to elevated blood pressure. In the assessment of HCM, the algorithm was applied to three groups of patients: sarcomere mutation carriers with overt HCM (G+/LVH+), sarcomere mutation carriers with subclinical HCM (G+/LVH-), and healthy controls (G-/LVH-). Additionally, we compared our algorithm with conventional echocardiographic measurements in all analyses. Overall, we sought to (1) demonstrate a relationship between sonographic signal intensity and myocardial microstructural alterations, (2) expand the algorithm's ability to distinguish the presence and extent of cardiac changes in response to elevated afterload stress in both mice and humans, and (3) investigate the algorithm's ability to distinguish between healthy individuals and sarcomere mutation carriers with overt and subclinical HCM.

Methods

Development and Standardization of Image Analysis Algorithm

Development of the Image Analysis Algorithm

A computational method of analysis was developed using the ImageJ software platform v1.46 (NIH, Bethesda, MD) to perform measurements of signal intensity distributions within 2D ultrasound images. An ImageJ macro was specifically designed to analyze a user-selected region-of-interest (ROI) within an 8-bit DICOM echocardiographic image or an 8-bit .jpg image, with individual pixels ranging from 0 to 255 intensity.[52]

Signal distribution analysis involves four steps (**Figure 2**): 1) image selection and formatting, 2) ROI sampling, 3) algorithm application, and 4) processing final values to yield a representative marker of myocardial microstructure. The algorithm functions to hierarchically re-order grayscale values of pixels within the region of interest, and then provide characteristics of the signal intensity distribution (**Figure 3**). Processing of raw data collected using the ImageJ software program was performed using MATLAB v8.0 (MathWorks, Natick, MA).

During development of the algorithm, the size of the region of interest values was incrementally adjusted, and the results of these adjustments were analyzed and compared. Development of the protocol included testing normalization of ROI values to internal reference parameters including pericardial intensity, signal distribution of the heart region, and signal distribution of the captured screen. Development of the protocol also included analysis of consecutive frames of echocardiographic image over the cardiac cycle.

Standardization of the Image Analysis Algorithm

The user protocol was standardized and included anatomical markers to define location and placement of the ROI. Each ROI had a standardized position with respect to each subject's

anatomical structures. The general region of interest was defined as the inferolateral basal segment of the LV in the parasternal long-axis view; the specific region of interest was defined as the pericardium adjacent and parallel to the mid-section of the inferolateral basal segment of the myocardium. A marker of myocardial microstructure selected from the signal distribution, termed the Signal Intensity Coefficient (SIC), was calculated as (1-p/256), where p is the 25th percentile of pericardial signal intensity distribution. User inter-and intra-reader variability was determined for multiple iterations of the protocol.

Conventional Echocardiographic Measures

In addition to the advanced image analyses described above, in all studies we also obtained conventional echocardiographic measures of structure and function including: LV wall thickness (LVWT) calculated as interventricular septum width plus posterior wall width, LV end-diastolic diameter (LVDD), LV end-systolic diameter (LVSD), LV mass, LV fractional shortening (FS), LV ejection fraction (calculated from the aforementioned linear measurements using the Teichholz method),[53] peak E prime velocity (lateral annulus), peak transmitral E velocity to A velocity ratio, and peak transmitral E velocity to peak E prime velocity ratio. The mean values across three cardiac cycles was used to determine the above measurements of cardiac dimensions and function. The average of tissue Doppler myocardial velocities at the inferior, septal, lateral, and anterior aspects of the mitral annulus was used to calculate global E prime velocity values. The relative wall thickness (RWT) was calculated as LVWT divided by LVDD.

Distinguishing Hypertensive Heart Disease in Mouse Echocardiograms

Experimental Model and Imaging Acquisition

We studied a cohort of 12 adult mice (C57/BL6, Jackson Laboratory) that were housed in a climate controlled facility with 12-hour alternating light cycles and access to food and water ad libitum. All animals were studied over a period of 7 weeks, after being randomized into one of the following 3 groups: vehicle control with sham operation at baseline (N=3), ascending aortic constriction applied surgically at baseline (N=4), and ascending aortic constriction applied surgically at baseline with subsequent removal of the aortic band at 3 weeks (N=3). Details regarding the experimental protocol, including the surgical aortic banding procedures, have been described previously.[54] At 7 weeks, all mice underwent echocardiographic image acquisition using a 28 MHz transducer with digital image capture (Vevo2100 Visualsonics, Toronto, ON) according to a standardized protocol.[55] All images underwent quality review then advanced image analysis, including calculation of the SIC, in a blinded fashion.

Histological Assessment

At 7 weeks, following echocardiography, mice were euthanized for pathological assessment of myocardial fibrosis. Histologic quantification of myocardial fibrosis was performed using a previously described automated image-analysis method (ImageJ, v1.46, Bethesda, MD).[56] Subject-based variability in echocardiographic images was determined by measuring the differences between multiple genetically identical mice at baseline. All animal procedures were approved by the Harvard Medical Area standing Institutional Animal Care and Use Committee.

Statistical Analyses

For the experimental study, we assessed differences in LV mass, RWT, and SIC at 7 weeks across all animal groups using the Kruskal-Wallis test, and between pairs of groups using

the two-sided Student's t-test. All analyses were performed using Stata SE (v12.1, StataCorp, College Station, TX), and a 2-sided P value <0.05 was considered statistically significant.

Distinguishing Human Hearts Exposed to Afterload Stress in Hypertensive Heart Disease

Study Sample and Clinical Data Acquisition

From a database of routine echocardiographic studies performed on patients referred to our institution's clinical laboratory, we selected echocardiograms from normotensive healthy controls (N=28) and individuals with hypertension (N=30) without diabetes or prevalent cardiovascular disease (i.e. free of coronary disease, heart failure, or prior cerebrovascular event). Data on clinical characteristics were extracted from electronic medical record, including blood pressure measurement performed on the day of or closest to the date of echocardiographic image acquisition (within 45 days). The following blood pressure measurements were recorded: systolic blood pressure (SBP), diastolic blood pressure (DBP), and mean arterial pressure (MAP) calculated as DBP plus (SBP-DBP)/3. All patient records and information were anonymized and de-identified prior to analyses. All clinical research protocols and procedures were approved by the institutional review board of the Brigham and Women's Hospital.

Imaging Acquisition and Echocardiographic Measurements

All images underwent review, while blinded to clinical data, for image quality and appropriateness for image analysis (based on visualization of the endocardial border in relation to the LV cavity and adjacent structures). In addition to conventional echocardiographic measures as described,[57] the advanced image analysis algorithm (including calculation of the SIC) was performed on all images in a blinded fashion.

Statistical Analyses

We compared clinical and echocardiographic characteristics of normotensive versus hypertensive individuals using the two-sided Student's T-test for continuous variables and the chi-square test for categorical variables. We then used regression analyses to examine the association of both conventional and advanced echocardiographic parameters (including the SIC) with hypertension status (present versus absent). In addition to unadjusted models, we performed regression analyses adjusting for age and sex. We also examined the association of conventional and advanced echocardiographic measures with increasing tertiles of each BP measure (SBP, DBP, and MAP). Additionally, in the total sample of individuals studied, we used regression analyses to examine the association of variation in SBP, DBP, and MAP with both conventional and advanced echocardiographic measures of LV structure (including the SIC). All analyses were performed using Stata SE (v12.1, StataCorp, College Station, TX), and a 2-sided P value <0.05 was considered statistically significant.

Distinguishing Human Hearts Exposed to Afterload Stress in HCM

Study Sample and Clinical Data Acquisition

Genotyped individuals with HCM were identified, and study participants were classified into three status groups. Overt HCM patients (G+/LVH+, N=10) included sarcomere mutation carriers with maximal LV wall thickness above 12mm. Subclinical genotype positive patients (G+/LVH, N=10) including sarcomere mutation carriers with maximal LV wall thickness less than or equal to 12mm. Healthy controls (G-/LVH-, N=10) included genotype negative individuals without myocardial hypertrophy or comorbidities. The following exclusion criteria were applied to all members of the cohort: systemic hypertension, coronary heart disease, presence of a permanent pacemaker, contraindication to gadolinium administration, infiltrative or

storage disease, and atrial fibrillation. The study design was created in the context of collaboration with authors of a previously published study.[11]

Imaging Acquisition

Cardiac magnetic resonance imaging acquisition was performed, as described previously,[11] using a 3.0 Tesla system (Tim Trio, Siemens, Erlangen, Germany). LV mass and LV function characteristics were calculated upon tracing the LV myocardial, epicardial, and endocardial borders on short-axis consecutive cine images at end-diastole and end-systole. Summation-of-discs method was used for LV mass calculation. LV wall thickness was measured in lateral, inferior, posterior, and anterior septal segments in all participants.

Late gadolinium enhancement (LGE) imaging was performed for detection of focal myocardial fibrosis. The LGE imaging protocol employed a segmental inversion-recovery pulse sequence, and the LGE quantification method utilized a semi-automated grayscale threshold technique. LGE was expressed in grams and as a percentage of total myocardial mass. LGE analyses were performed using commercially available software (QMassMR, version 7.4, Medis, Leiden, The Netherlands). Myocardial ECV was calculated through a previously established algorithm.[11] For participants with regional fibrosis detected by LGE, a second ECV value was calculated after excluding regions that contained LGE.

Echocardiographic image acquisition was performed within average 41±94 days of CMR imaging. The Vivid-7 ultrasound system was used to obtain standard echocardiograms and tissue Doppler interrogation (GE Medical System, Milwaukee, WI). Conventional echocardiographic imaging characteristics and the microstructural echocardiographic assessment of SIC were obtained as described in methods above. All echocardiographic measurements were performed while blinded to genotype and clinical information.

Biomarker Assessments

Serum biomarker measurements were performed through collection of peripheral blood at the time of cardiac MRI imaging.[11] Biomarkers included amino terminal pro-peptide of B-type natriuretic peptide (NT-proBNP, Roche, Indianapolis, IN), supersensitive cardiac troponin (TnI, Singulex, Atlanta, GA), and carboxy-terminal propeptide of procollagen type I (PICP, Quidel Corporation, San Diego, CA). All assays were performed using commercially available reagents, in a blinded fashion.

Statistical Analyses

Clinical, echocardiographic, and MRI characteristics were assessed across the three HCM status groups. Logistic regression with clustering was used to account for familial relationships, and analyses were adjusted for family relationship as well as age and sex. Pearson correlation was used to obtain associations between continuous measures. Kruskall-Wallis test was used to evaluate differences between pairs of groups. Based on comparisons made across three groups, a two-tailed P-value of 0.05/3=0.017 was considered to be statistically significant. All analyses were performed using STATA v12.1 (StataCorp, College Station, TX).

Results

Development and Standardization of Image Analysis Algorithm

Analyses of pericardial, myocardial, and full-region signal distributions in mice and humans revealed patterns in the data (**Figure 4**). More echogenic (i.e. brighter) areas such as the pericardium demonstrated a right-shifted distribution. Smaller and/or more homogeneous areas demonstrated a narrower distribution. Parallel analyses in mice and humans revealed similar results, suggesting that patterns in the data are species-independent, and that trends are strongly dependent upon grayscale patterns formed by tissue microstructure.

Signal analyses were expected to reveal changes in grayscale signal distribution throughout the cardiac cycle, corresponding to the anticipated decrease in myocytes per area during myocardial wall relaxation in diastole compared to systole. Cyclic variability, as demonstrated in **Figure 5**, shows signal intensity variation in mice with 7 weeks ascending aortic constriction and mice that underwent sham surgery. As expected, the myocardial grayscale signal intensity is lowest in the end-diastolic frame. Furthermore, it is observed that higher percentiles of the signal (80th percentile) demonstrate greater relative variability compared to lower percentiles of the signal (20th percentile).

Analyses of reproducibility accounted for the influence of anatomical structures, ROI size, and imaging references upon baseline variability, cyclical variability, and intra-user reproducibility (**Table 2**). It was observed that use of a regional ROI was associated with high cyclical variability and high baseline variability, compared to use of the full myocardial region. Use of a large ROI was associated with lower baseline variability, high cyclical variability, and higher intra-user reproducibility ($R = 0.87$-0.97) compared to use of a small ROI. Use of a reference region, such as a myocardial-to-pericardial ratio, resulted in higher baseline variability

compared to use of grayscale intensity values without a reference. The algorithm selected to produce SIC values utilized a pericardial reference area that maximized intra-user reproducibility and inter-user reproducibility (R = 0.90 and 0.89, respectively), minimized baseline variability (24-29%), and demonstrated moderate cyclical variability.

Distinguishing Myocardium Exposed to Afterload Stress in Mice

After 7 weeks of the experimental protocol, echocardiographic images were acquired and analyzed for all 3 animal groups: mice that underwent the sham surgery (control), mice that underwent ascending aortic constriction at baseline and then debanding at 3 weeks (debanded), and mice that underwent ascending aortic constriction at baseline without further intervention (banded). With respect to conventional echocardiographic parameters (**Figure 6**), measures of LV mass differentiated between debanded and banded mice (P=0.008), but not between control and debanded mice (P=0.60) or across the 3 groups overall (P=0.053). There was no significant difference between animal groups with respect to RWT (P≥0.73). By contrast, the SIC was significantly different across all 3 groups of mice (P=0.026) and also differentiated between control and debanded (P=0.015) as well as between banded and debanded mice (P=0.031). At the end of the protocol, mice from the control, debanded, and banded groups were sacrificed and histologic examination showed evidence of greater fibrosis in debanded compared with control mice, and greater fibrosis in banded compared to debanded mice (**Figure 7**). Image analysis-based automated quantification of myocardial fibrosis from representative Masson's trichrome stained sections demonstrated fibrosis scores of 3.2%, 8.1%, and 23.3% for control, debanded, and banded mice, respectively. All echocardiographic measures were highly correlated with quantitation of fibrosis: r=0.95 for LV mass, r=0.72 for RWT, and r=0.92 for SIC.

Distinguishing Myocardium Exposed to Afterload Stress in Humans

Clinical and echocardiographic characteristics for individuals in the healthy control group (N=28) compared with individuals in the hypertensive group (N=30) are shown in **Table 3**. There was no significant difference in age or sex when individuals in the healthy control group were compared to those in the hypertensive group (P≥0.24). As expected, all BP measures were significantly higher in the hypertensive group. With respect to echocardiographic traits, there was no significant difference between groups in conventional measures of LV structure and systolic function; the conventional measures of diastolic function, E prime and E/e' ratio, were worse in hypertensive individuals than controls, as expected (**Table 3**). The novel measure of myocardial microstructure, SIC, was also significantly higher in hypertensive individuals compared with normotensive individuals (P=0.029). Accordingly, in regression analyses (**Table 4**), conventional echocardiographic parameters were not significantly associated with hypertensive status in models with and without adjustment for age and sex, with the exception of E prime and E/e' ratio. Notably, higher values of SIC (P=0.029) was also associated with hypertension in unadjusted models; these associations remained significant in models adjusting for age and sex.

In analyses of variation in BP across all the individuals studied, there was no significant association of SBP, DBP, or MAP with LV mass (**Figure 8**). Although higher MAP was associated with higher RWT (P=0.043), there was a borderline significant association of DBP with RWT (P=0.052) and there was no significant association of SBP with RWT (P=0.42). Notably, higher levels of SBP were also not significantly associated with the SIC in these unadjusted analyses. However, increasing DBP was associated with higher measures of the SIC (P=0.020). Similarly, increasing levels of MAP was also associated with higher values of the SIC (P=0.017).

In regression analyses examining the relation of BP indices with echocardiographic traits, there were no significant associations of BP with the following conventional measures of structure: LV size, wall thickness, or mass (**Table 5**). The only associations observed between BP and any conventional measures included RWT with MAP (P=0.02), and E prime with SBP (P=0.03). By contrast, increasing values of SBP, DBP, and MAP were all significantly associated with the SIC measure (**Table 5**). These associations all remained significant in analyses adjusting for age and sex (P<0.05 for all), with the exception of a borderline significant relation of SBP with SIC (P=0.053).

Characterizing Myocardial Disease in Subclinical and Clinical HCM

Clinical characteristics within the study sample included age and sex (**Table 6**). Individuals with overt HCM were more likely to be male (P=0.003). Furthermore, individuals with overt HCM (G+/LVH+) were older than individuals with subclinical HCM (G+/LVH-; P=0.09)) and were significantly older than healthy controls (P=0.006).

Analyses of conventional imaging parameters and biomarkers were adjusted for age, sex, and familial relations (**Table 6**). Serum biomarkers (PCIP, TnI, NT-proBNP) did not demonstrate significant differences in biomarker levels between mutation carriers and healthy controls. However, biomarkers PICP and Singulex TnI demonstrated significant differences between overt HCM and subclinical HCM subgroups (P=0.006 for PICP and P=0.008 for Singulex TnI). The SIC was moderately correlated with serum biomarkers in a cohort of individuals with overt, subclinical, and HCM (r=0.50 for Singulex TnI, r=0.50 for NT-proBNP) (**Table 7**). Conventional echocardiographic measures of LV mass and maximum LV wall thickness were significantly different between the overt and subclinical HCM subgroups, but were not significantly different between the subclinical and control HCM subgroups. Left

ventricular ejection fraction did not demonstrate significant differences between any comparisons. Of the conventional imaging measures, only global E' velocity showed significant differences between overt and subclinical subgroups, as well as between the subclinical subgroup and healthy controls (**Figure 9**).

With respect to microstructural measurement methods, LGE was present and measurable only in the overt HCM subgroup. By contrast, SIC and ECV were measurable in all subgroups. In analyses adjusted for age, sex, and familial relationship (**Table 6**), ECV was on average 35 percent higher in individuals with overt HCM compared to healthy controls (P<0.0001), and ECV was on average 14.5 percent higher in individuals with overt HCM compared to individuals with subclinical HCM (P=0.005). In parallel, SIC was on average 62 percent higher in individuals with overt HCM compared to healthy controls, and SIC was on average 32 percent higher in individuals with overt HCM compared to subclinical HCM (P<0.0001 for both). Both ECV and SIC distinguished between different pairs of subgroups in a statistically significant manner (**Figure 9**).

In analyses of correlations in the total study sample (**Table 7**), SIC demonstrated significant correlations with echocardiographic maximum LV wall thickness, LV mass, echocardiographic global E' velocity, and ECV. In comparison, ECV demonstrated significant correlations with SIC, LGE, and global E' velocity; of these, ECV had the highest correlation with SIC (R=0.84, P<0.001). For patients with measurable LGE, the correlation of LGE with ECV (R=0.75, P=0.03) was strong and statistically significant, whereas the correlation of LGE with SIC was weak and was not statistically significant (R=0.38, P=0.36). Global E' velocity correlation with SIC (R=-0.84, P<0.001) was stronger than global E' velocity correlation with ECV (R=-0.70, P<0.001). Maximum LV wall thickness also demonstrated stronger correlation with SIC (R=0.61, P<0.001) compared to ECV (R=0.39, P=0.04).

Discussion

We developed an ultrasound-based image analysis algorithm to assess microstructural characteristics of LV myocardium. We evaluated our algorithm in two disease states that typically involve progressive cardiac remodeling from microstructural to macrostructural changes: (1) hypertensive heart disease, and (2) HCM. The novel algorithm was first applied to cohorts exposed to varying degrees of afterload stress: a mice cohort with aortic banding to simulate afterload stress, as well as a human cohort with varying degrees of blood pressure. Next, the algorithm was applied to a cohort of sarcomere mutation carriers with overt and subclinical HCM as well as healthy controls. The signal intensity coefficient (SIC) marker produced by our algorithm was compared with conventional echocardiographic parameters of adverse LV remodeling, tissue histology, and an MRI-based microstructural measure of fibrosis (ECV).

First, we observed that the SIC, an indirect measure of LV microstructure, was significantly higher in hypertensive compared to non-hypertensive myocardium in both our clinical study and experimental model. Second, the SIC was positively related to increasing levels of blood pressure exposure in humans as well as to increasing levels of afterload stress in mice. Third, we also observed in humans that the SIC demonstrated stronger associations with hypertension status and degree of blood pressure elevation compared to established echocardiographic measures of adverse LV remodeling. Fourth, in a cohort of sarcomere mutation carriers and healthy controls, the SIC demonstrated strong associations with the MRI-based ECV measure, as well as with LV mass and myocardial relaxation velocity. Finally, both the ECV and SIC were able to distinguish between individuals with overt HCM, subclinical HCM, and healthy controls.

Overall, our results demonstrate the potential of an imaging algorithm to identify the presence and extent of microstructural changes that can arise early in the development of adverse LV remodeling in response to chronic exposure to afterload stress as well as genetic mutations.

Role of SIC in Assessment of Early Cardiac Remodeling

The SIC appears to demonstrate ability to distinguish microstructural changes in early stages of cardiac remodeling, as seen in hypertensive myocardium of mice and humans and in sarcomere mutation carriers with different phenotypes of HCM.

When applied to mouse echocardiograms, the SIC measurement was able to differentiate between control and debanded, as well as between debanded and continuously banded, animals. In effect, the SIC was able to identify differences between animals exposed to mild versus moderate, as well as moderate versus high, levels of chronic afterload resistance. Conversely, conventional echocardiographic measures of gross morphology (i.e. 'macrostructure'), such as LV mass, only distinguished between controls and animals exposed to the highest levels of chronic afterload resistance.

Consistent with our findings in mice, the individuals with hypertension in our clinical study were otherwise healthy and were similar to normotensive controls with respect to age and sex. Thus, the clinical cohort included younger to middle-aged individuals, in whom elevations in DBP are known to be more common than elevations in SBP.[23, 58] Accordingly, we observed that the SIC was more prominently associated with DBP and MAP rather than with SBP. Similar findings were seen for RWT, although these associations were not statistically significant. Thus, the SIC appears more sensitive to myocardial changes that are likely to occur during the earliest stages of variation in blood pressure. Taken together, our findings suggest that the SIC measure could serve as a sensitive marker of LV microstructure that complements conventional

echocardiographic techniques for assessing the presence and severity of cardiac remodeling changes that arise along the spectrum of hypertensive heart disease.

In genotype-positive individuals with overt and subclinical HCM, our study findings suggest that the SIC may act as a non-invasive measure of tissue-level changes prior to macrostructural changes. Neither LV mass nor wall thickness differed between phenotype-negative sarcomere mutation carriers and healthy controls, by definition. However, the SIC was seen to be significantly higher in the G+/LVH- group, further supporting the finding that sarcomere mutation carriers may have tissue-level pathology in the absence of overt structural alterations in the myocardium.

Results in both hypertensive heart disease and HCM support the potential for SIC to serve as a sensitive marker of early microstructural changes, prior to development of global changes. Cardiac remodeling pathways in both HCM and hypertensive heart disease involve a combination of multiple microstructural changes, which may yield mixed influences upon the signal distribution. For instance, fibrosis and cellular elongation may be present within both HCM and hypertensive heart disease, but these features may manifest heterogeneously at different time points, to varying degrees, or in distinct spatial patterns within the tissue.[5] In order for the SIC to provide more disease-specific information, further studies are needed to characterize the nature of microstructural changes involved in cardiac remodeling pathways of HCM and hypertensive heart disease.

Comparison with Tissue Histology

The SIC is a non-invasive measurement, inherently providing an advantage over invasive approaches toward tissue analyses. Histology, the gold standard for tissue characterization, requires sacrifice of mice in experimental studies and costly invasive procedures in humans.

Study findings demonstrate that the SIC may provide complementary tissue assessment through non-invasive methods. In our experimental model of mice exposed to varying levels of afterload stress, Masson trichrome stains demonstrated a strong positive correlation between fibrosis and SIC. Although non-invasive imaging may not offer the degree of specificity that is available in histological assessment, the SIC has the advantage of providing quantitative non-invasive microstructural information. Thus, the SIC demonstrates potential for use as an adjunctive tool in tissue analyses.

Comparison with Cardiac Biomarkers

Conventional serum biomarkers, which require serum measurements as opposed to tissue samples, have limited sensitivity and specificity in characterization of HCM.[20] The SIC was moderately correlated with serum biomarkers in a cohort of individuals with overt, subclinical, and HCM. Although serum biomarkers did not demonstrate significant differences between phenotype-negative sarcomere mutation carriers and healthy controls, the SIC was able to distinguish between all three subgroups. These results suggest that the SIC may be more sensitive to early disease changes compared to serum biomarkers.

Comparison with Conventional Echocardiographic Parameters of Cardiac Remodeling

The present studies extend prior work by comparing and integrating established measures of structural heart disease with ultrasonic measures of LV myocardial microstructure. Although conventional structural echocardiographic measures, such as LV mass and wall thickness, are known to reflect worsening degrees of cardiac remodeling, the associations of these gross morphologic parameters with blood pressure exposure and sarcomere mutations are non-linear and complex.[20, 59] Because microstructural changes are likely to precede macrostructural changes

within the myocardium, a microstructural marker has the potential to identify adverse myocardial remodeling, at early stages of disease and with increased sensitivity.

Accordingly, in our studies of afterload stress and sarcomere mutations, we observed particularly significant associations of the SIC with early cardiac changes compared to conventional echocardiographic measures of cardiac structure. LV mass did not distinguish between groups of mice exposed to increasing levels of afterload stress, nor between increasing tertiles of blood pressure within the human cohort. By contrast, the SIC demonstrated a significant difference between all subgroups. Although RWT demonstrated a positive trend with increasing levels of afterload stress in both humans and mice, the SIC provided stronger statistical significance when differentiating between these groups. Parallel results in the HCM study demonstrated that conventional structural echocardiographic measures of LV mass and absolute wall thickness were unable to differentiate between the subclinical HCM subgroup versus healthy controls. By contrast, the SIC was significantly different between all three subgroups. Nevertheless, conventional structural parameters were positively associated with the SIC, as seen in the HCM study. The SIC was particularly strongly correlated with maximum LV wall thickness. This may be explained by the mechanism of the algorithm, which utilizes a measurement through the length of the LV myocardium in the parasternal axis, and effectively captures an indirect measurement of LV wall thickness.

Unlike conventional structural measures, conventional functional parameters of adverse remodeling were successful in distinguishing between select subgroups in the clinical study of afterload stress and in the HCM study. Global E' velocity, a measurement of diastolic function, demonstrated a significant difference between hypertensive and non-hypertensive individuals (P=0.0002). However, unlike the SIC, global E' velocity was found to be significantly different between tertiles of SBP but not between tertiles of DBP and MAP. In the HCM study, global E'

velocity performed similarly to the SIC by demonstrating a statistically significant difference between sarcomere mutation carriers versus healthy controls. The relationship between myocardial microstructure and diastolic function in the pathogenesis of HCM[8, 12, 15] is additionally supported by the finding of a strong inverse correlation between SIC and global E' velocity (R=-0.84, P<0.01). Previous echocardiographic techniques have attempted to use strain imaging to characterize functional changes in HCM, as opposed to characterization of structural tissue changes.[10, 60] However, in the setting of early heterogeneous tissue changes, the relationship between structure and function in early remodeling is unclear. If microstructural techniques such as the SIC were to be combined with functional measures such as global E' velocity, an aggregate measure might have the potential to characterize a wider spectrum of cardiac remodeling changes.

Comparison with CMR-based Microstructural Measures

CMR-based ECV measurements have previously been established as non-invasive markers of myocardial fibrosis in HCM pathogenesis.[8, 11, 13] The ability of both ECV and SIC to differentiate between all three phenotypic subgroups is evident in our results. Furthermore, the SIC was strongly correlated with ECV. Although grayscale sonographic signal distributions may be influenced by an array of tissue changes, our findings suggest that the SIC may also act as a marker of interstitial myocardial fibrosis in HCM. However, ECV and SIC differed in the strength of associations with other HCM assessment parameters. Most notably, LGE demonstrated stronger correlation with ECV compared to SIC, whereas LV wall thickness was more strongly associated with SIC compared to ECV. These differences may arise from the position-dependence of the SIC measure. For a given image, the ROI used to calculate the SIC may be situated in an anatomical location distinct from the anatomical location of the LGE,

thereby limiting the influence of the LGE upon the SIC. Moreover, myocardial tissue properties may variably influence ECV and SIC, since ECV measures extracellular volume[11] whereas SIC measures aggregate microstructural features.[52]

Despite differences between the SIC and ECV, our data suggest that SIC and ECV provide complementary results and may be used together to quantify severity of adverse remodeling in HCM. The SIC may also provide an inherent advantage over CMR-based ECV due to reduced image acquisition time, absence of required intravenous contrast, and reduced costs. Of note, investigators have previously attempted to use echocardiography to calculate fibrosis in HCM, but these methods utilized strain echocardiography as opposed to microstructural tissue analysis.[10, 15] The role of SIC and/or ECV in predicting adverse outcomes in HCM has yet to be determined.

Comparison to Previously Developed Sonographic Microstructural Measures

The image analysis algorithm used to produce the SIC measure differs in several ways from similar algorithms employed in prior studies.

First, the SIC is based on the 25th percentile of the signal distribution in the region of interest. Many published techniques for assessing myocardial microstructure have relied on mean grayscale values, obtained through integrated backscatter or comparable signal analysis methods. However, other studies have suggested that using the complete distribution of signal intensity values allows for a more sensitive and specific assessment of signal changes compared with use of only the mean signal intensity value.[40, 48, 61-64] Ciulla et al. demonstrated that kurtosis and other measures of signal distribution were positively correlated with collagen content in hypertensive patients.[65] In a similar fashion, a percentile value of signal intensity offers information regarding

the widening or shift of a signal distribution, in addition to allowing for quantitative comparisons between measures.

Second, the SIC measure represents signal intensities within a pericardial region of interest. Prior studies have traditionally assessed the myocardium, alone or standardized to the pericardium.[46, 63, 66-71] Cyclical variation of the myocardial signal (i.e. standardization of a myocardial measure in one frame compared with another) has also been assessed.[42, 51, 66, 72, 73] Use of a pericardial region of interest extends from these prior methods given the fact that ultrasound signal reaching and reflected by the pericardium is dependent upon its transmission through the adjacent myocardium. Thus, in the standard orientation of sonographic transduction in the long axis view, the pericardial signal is a function of the post-myocardial signal.

Third, the SIC provides greater accessibility compared to previous techniques. Unlike prior methods requiring proprietary equipment,[74-77] novel acquisition modalities,[77-80] or complex time-intensive data processing,[38-40, 81] the SIC uses open-source software, and utilizes protocols that can be applied retrospectively and prospectively using multiple file formats.

Possible Mechanisms Underlying the Measurement of SIC

The exact mechanism by which the SIC measure is able to differentiate between states of afterload resistance, as well as different HCM genotypes and phenotypes, is not entirely clear. Studies of microstructural image analysis have long sought to understand how pathologic changes of the myocardium manifest as sonographic signal intensity variation. Prior investigators using echocardiographic analyses of tissue have suggested that pathologic compared with non-pathologic changes within the LV wall can effectively change tissue impedances, thereby altering sonographic signals. Several studies have noted that cyclic variation in mean gray levels of integrated backscatter signals, which normally increase at end-diastole and decrease at end-

systole, show less variation in the setting of hypertension and coronary disease.[31, 32, 82, 83] Tissue-level characteristics that influence ultrasonic backscatter are thought to include collagen content and fibrosis, tissue heterogeneity, fiber orientation, wall thickness, cell size, and sarcomere length.[31, 65, 82, 84] The features that influence ultrasonic backscatter are also features involved in cardiac remodeling changes. Interestingly, histologic changes have been associated with both increases and decreases in signal intensity. Increased signal intensity has been attributed specifically to wall thickness and increase myocyte size and density.[30] Leftward shifts in (i.e. decreased) signal intensity have been attributed to heterogeneously increased collagen content and fiber disorientation that can cause constructive and destructive signal interactions with diffuse signal scattering.[65]

In the present study, the positive correlation observed between SIC and increasing stages of myocardial disease indicate that a pre-specified percentile value of pericardial signal intensity decreases with increasing levels of adverse remodeling. Signal that is more diffusely scattered due to increased tissue heterogeneity and fiber disarray may demonstrate lower signal intensity upon reaching the interface of the myocardium and pericardium. Alternatively, signal that is reflected in the myocardium more proximally, due to collagen or calcium deposits, may also result in reduced pericardial intensities. This kind of "acoustic speckle" effect has been described previously[29] and may be similar to the acoustic shadowing effects seen in ultrasound imaging studies of vascular atherosclerosis.[75, 81] Additionally, it is possible that certain microstructural features influence the signal intensity more than others. Distinct microstructural changes may appear at different stages during the progression of hypertensive heart disease, potentially contributing to the inconsistent findings reported by prior studies of myocardial signal intensity in the setting of hypertension. Thus, analysis of the myocardium may be affected by both scattering effects that reduce the signal and increased echogenicity of structures that increase the

signal. By contrast, the pericardial signal is likely to reflect only the changes due to scattering, yielding a uniformly lower signal. Further studies are needed to elucidate the exact mechanisms by which the pericardial value appears to consistently decrease and, in turn, the SIC is observed to consistently increase in relation to progressive cardiac remodeling.

Potential Applications

The SIC has the potential to serve as a quantitative marker of myocardial disease severity in the assessment of hypertensive heart disease and HCM in humans, including changes in myocardial structure over time and responses to treatment. Advantages of the SIC include wide accessibility and ease of use through open access software that can be applied to routinely acquired echocardiographic images. Although further evaluation in more diverse clinical cohorts is needed, our initial results in human cohorts and an animal model suggest that the SIC may be particularly robust to variation in image acquisition settings and physiology. As a measure of cardiac microstructure, the SIC may also be used to differentiate severity of myocardial pathology in non-hypertensive and non-HCM disease states. Further studies are needed to assess the extent to which the SIC correlates with histologic changes in myocardial microstructure during the course of adverse remodeling. Further studies are also needed to assess the potential utility of the SIC in broader clinical contexts. In addition to potential clinical applications, validated microstructural image analysis techniques may be used as adjunctive tools for investigating the pathophysiology of hypertensive heart disease and HCM. Hypertensive heart disease and HCM are both recognized as complex diseases having multiple subclinical and clinical disease manifestations.[59] Thus, microstructural imaging techniques could be used to further study the time course and nature of cardiac remodeling in more diverse clinical cohorts. Future studies may include additional algorithm development to elucidate disease-specific

patterns within the signal distribution. Algorithm development may include assessing grayscale intensity gradients and textural features within the myocardium and pericardium, establishing a consistent baseline reference and/or ROI selection process, and machine learning algorithms in the setting of larger sample sizes and standardized images.

Limitations

The imaging algorithm has a number of technical limitations that merit consideration. The algorithm is limited to images without artifacts, as these might interfere with ROI selection. Images must have adequate visualization of the endocardial border and sufficient overall quality in order to facilitate ROI selection. When insufficient dynamic range is employed, the algorithm may be unable to create an appropriate signal distribution. Although such instances are rare, studies of new phenotypes and/or images using unconventional acquisition techniques would benefit from preliminary assessment of backscatter linearity and dynamic range. Other notable technical limitations include lack of automation of the ROI, and possibly limited capacity for cross-comparison of markedly different echocardiographic acquisition parameters. Further studies are required to determine the need for revised protocols when addressing images acquired using different echocardiographic equipment.

Several limitations of the clinical and experimental studies merit consideration. Our study designs were retrospective, although all analyses were performed while blinded to clinical characteristics. Since blood pressure is known to be difficult to measure in mice,[85] banded versus debanded status was used as a surrogate measure of variation in chronic afterload resistance in the experimental model. The clinical studies were limited by inability to obtain tissue samples for comparison with fibrosis and other tissue changes. Furthermore, generalizability to populations of varying age group, race, and comorbidities remains unknown and may be the

subject of future investigations. Additionally, our human study sample sizes were small, particularly in the HCM cohort. Although findings in these small-sized cohorts did demonstrate significant associations, further studies in larger samples are warranted.

Summary

We developed and evaluated a novel ultrasound-based image analysis algorithm designed to differentiate microstructural characteristics of LV myocardium. The algorithm analyzes sonographic post-myocardial signal distributions arising from grayscale intensities within a pericardial region of interest, and produces a marker termed the signal intensity coefficient (SIC), which can serve as an enhanced surrogate measure of myocardial microstructure.

We evaluated our algorithm in two disease processes that are characterized by progressive LV remodeling from microstructural to global myocardial changes: (1) hypertensive heart disease, and (2) hypertrophic cardiomyopathy. We first evaluated our algorithm in cohorts exposed to varying degrees of afterload stress: a mice cohort with ascending aortic banding to simulate afterload stress, as well as a human cohort with varying degrees of blood pressure. Next, we evaluated our algorithm in sarcomere mutation carriers with overt and subclinical HCM. The SIC marker was compared with conventional echocardiographic parameters of adverse LV remodeling, mice tissue histology, and an MRI-based microstructural measure of fibrosis termed the ECV.

Results demonstrate that the SIC was significantly higher in hypertensive compared to non-hypertensive myocardium in both mice and humans, and was positively associated with increasing levels of exposure to afterload stress in humans and in mice. Furthermore, in a cohort of sarcomere mutation carriers with different phenotypes of HCM, the SIC was able to distinguish between individuals with overt HCM, subclinical HCM, and healthy controls. The SIC demonstrated stronger associations with both degree of blood pressure and MRI-based ECV compared to established echocardiographic measures of adverse LV remodeling.

Overall, our results demonstrate the potential of an imaging algorithm to identify the presence and extent of microstructural changes that can arise early in the development of cardiac remodeling, in response to chronic exposure to afterload stress as well as genetic mutations. The SIC appears to be more sensitive to early myocardial changes compared to conventional imaging methods and serum biomarkers, and may provide complementary information to other microstructural measures such as the ECV. Unlike prior echocardiographic tissue imaging methods, the SIC uses a pericardial region of interest, analyzes complete sonographic signal distributions, and is more accessible through open access software. Further studies are needed to assess the clinical utility of the SIC as a marker of adverse remodeling, and to understand the association of the SIC with disease-specific microstructural changes.

References

1.   Cohn JN FR, Sharpe N. Cardiac remodeling--concepts and clinical implications: a consensus paper from an international forum on cardiac remodeling. Journal of American College of Cardiology. 2000;35(3):569-82.

2.   Ahmad F SJ, Seidman CE. The genetic basis for cardiac remodeling. Annual Review of Genomics and Human Genetics. 2005;6:185-216.

3.   Athanasopoulos LV MS, Khalpey Z, Rawn JD, Schmitto JD, Wollersheim LW, Maloney AM, Cohn LH. Usefulness of preoperative cardiac dimensions to predict success of reverse cardiac remodeling in patients undergoing repair for mitral valve prolapse. American Journal of Cardiology. 2014;113(6):1006-10.

4.   Kehat I MJ. Molecular pathways underlying cardiac remodeling during pathophysiological stimulation. Circulation. 2010;122:327-34.

5.   Kessler EL BM, van Rijen HV, Vos MA, van Veen TA. Passive ventricular remodeling in cardiac disease: focus on heterogeneity. Frontiers in Physiology. 2014;5:482.

6.   Gradman AH AF. From left ventricular hypertrophy to congestive heart failure: Management of hypertensive heart disease. Progress in Cardiovascular Diseases. 2006;48(5):326-41.

7.   Wang TJ LD, Benjamin EJ, Vasan RS. The epidemiology of "asymptomatic" left ventricular systolic dysfunction: Implications for screening. Annals of Internal Medicine. 2003;138:907-16.

8.   Losi MA NS, Galderisi M, Betocchi S, Cecchi F, Olivotto I, Agricola E, Ballo P, Buralli S, D'Andrea A, D'Errico A, Mele D, Sciomer S, Mondillo S. Echocardiography in patients with hypertrophic cardiomyopathy: usefulness of old and new techniques in the diagnosis and pathophysiological assessment. Cardiovascular Ultrasound. 2010;8(7).

9.   Heidenreich PA AN, Allen LA, Bluemke DA, Butler J, Fonarow GC, Ikonomidis JS, Khavjou O, Konstam MA, Maddox TM, Nichol G, Pham M, Pina IL, Trogdon JG. Forecasting the impact of heart failure in the united states: A policy statement from the american heart association. Circulation Heart Failure. 2013.

10.   Almaas VM HK, Strøm EH, Scott H, Smith HJ, Dahl CP, Geiran OR, Endresen K, Aakhus S, Amlie JP, Edvardsen T. Noninvasive assessment of myocardial fibrosis in patients with obstructive hypertrophic cardiomyopathy. Heart. 2014;100(8):631-8.

11.   Ho CY AS, Neilan TG, Shah RV, Chen Y, Heydari B, Cirino AL, Lakdawala NK, Orav EJ, González A, López B, Díez J, Jerosch-Herold M, Kwong RY. T1 measurements identify extracellular volume expansion in hypertrophic cardiomyopathy sarcomere mutation carriers with and without left ventricular hypertrophy. Circulation Cardiovascular Imaging. 2013;6(3):415-22.

12.   Ho CY CC, Thune JJ, Havndrup O, Bundgaard H, Farrohi F, Rivero J, Cirino AL, Andersen PS, Christiansen M, Maron BJ, Orav EJ, Køber L. Echocardiographic strain imaging to assess early and late consequences of sarcomere mutations in hypertrophic cardiomyopathy. Circulation Cardiovascular Genetics. 2009;2(4):314-21.

13.   Ho CY LB, Coelho-Filho OR, Lakdawala NK, Cirino AL, Jarolim P, Kwong R, González A, Colan SD, Seidman JG, Díez J, Seidman CE. Myocardial fibrosis as an early manifestation of hypertrophic cardiomyopathy. New England Journal of Medicine. 2010;363(6):552-63.

14.   Afonso LC BJ, Bax JJ, Abraham TP. Echocardiography in hypertrophic cardiomyopathy: the role of conventional and emerging technologies. JACC Cardiovascular Imaging. 2008;1(6):787-800.

15.   Popović ZB KD, Mishra M, Buakhamsri A, Greenberg NL, Thamilarasan M, Flamm SD, Thomas JD, Lever HM, Desai MY. Association between regional ventricular function and myocardial fibrosis in hypertrophic cardiomyopathy assessed by speckle tracking echocardiography and delayed hyperenhancement magnetic resonance imaging. Journal of American Society of Echocardiography. 2008;21(12):1299-305.

16.   Drazner M. The progression of hypertensive heart disease. Circulation. 2011;123.

17.   Katz A. Maladaptive growth in the failing heart: the cardiomyopathy of overload. Cardiovascular Drugs and Therapy. 2002;16:245-9.

18.   Iwata M CR, Yeo SJ, Greenberg B. Targeting the ACE2-Ang-(1-7) pathway in cardiac fibroblasts to treat cardiac remodeling and heart failure. Journal of Molecular and Cellular Cardiology. 2011;51(4):542-7.

19.   Brown RD AS, Mitchell MD, Long CS. The cardiac fibroblast: therapeutic target in myocardial remodeling and failure. Annual Review of Pharmacology and Toxicology. 2005;45(657-687).

20.   Olivotto I CF, Poggesi C, Yacoub MH. Patterns of disease progression in hypertrophic cardiomyopathy: an individualized approach to clinical staging. Circulation Heart Failure. 2012;5(4):535-46.

21.   Wong M SL, Latini R, Barlera S, Glazer R, Aknay N, Hester A, Anand I, Cohn JN. Severity of left ventricular remodeling defines outcomes and response to therapy in heart failure: Valsartan heart failure trial (Val-HeFT) echocardiographic data. Journal of American College of Cardiology. 2004;43(11):2022-7.

22.   Vasan R. Biomarkers of cardiovascular disease: molecular basis and practical considerations. Circulation. 2006;113(19):2335-62.

23.   Cheng S, Xanthakis V, Sullivan LM, Vasan RS. Blood pressure tracking over the adult life course: patterns and correlates in the Framingham heart study. Hypertension. 2012;60(6):1393-9. Epub 2012/10/31.

24.   E B. Biomarkers in heart failure. N Engl J Med. 2008;358(20):2148-59.

25.   Spinale FG ZM. Integrating the myocardial matrix into heart failure recognition and managemen. Circulation Research. 2013;113:725-38.

26.   Schelbert EB FG, Bonow RO, Butler J, Gheorghiade M. Therapeutic targets in heart failure: Refocusing on the myocardial interstitium. Journal of American College of Cardiology. 2014;63:2188-98.

27.   Dorn G, Robbins, J, Sugden, PH. Phenotyping hypertrophy: eschew obfuscation. Circulation Research. 2003;92(1171-1175).

28.   Kapur N. Transforming growth factor-beta: Governing the transition from inflammation to fibrosis in heart failure with preserved left ventricular function. Circulation Heart Failure. 2011;4:5-7.

29.   Olshansky B CS, Skorton DJ, Prasad NV. Variation of left ventricular myocardial gray level on two-dimensional echocardiograms as a result of cardiac contraction. Circulation. 1984;70(6):972-7.

30.   O'Brien PD OBWJ, Rhyne TL, Warltier DC, Sagar KB. Relation of ultrasonic backscatter and acoustic propagation properties to myofibrillar length and myocardial thickness. Circulation. 1995;91(1):171-5.

31.   Maceira AM, Barba J, Varo N, Beloqui O, Diez J. Ultrasonic backscatter and serum marker of cardiac fibrosis in hypertensives. Hypertension. 2002;39(4):923-8.

32.   Yamada S, Komuro K. Integrated backscatter for the assessment of myocardial viability. Current opinion in cardiology. 2006;21(5):433-7. Epub 2006/08/11.

33.   Meunier J BM. Echographic image mean gray level changes with tissue dynamics: a system-based model study. IEEE Transactions on Biomedical Engineering. 1995;42(403-410).

34.   Hiremath P BM, Aguirre AD, Cheng H-W, Unno K et al. Identifying Early Changes in Myocardial Microstructure in Hypertensive Heart Disease. Plos One. 2014;9(5):e97424.

35.   Hiremath P BM, Cheng H, Unno K, Liao R, Cheng S. . Ultrasonic assessment of myocardial microstructure. . J Exp Vis. 2013;In Press.

36.   Raab P HE, Franz K, Friehelm E, Lanfermann H. Cerebral gliomas: diffusional kurtosis imaging analysis of microstructural differences. Radiology. 2010;254(3).

37.   Raz E BM, Sigmund EE, Tabesh A, Babb JS, Jaggi H, Helpern J, Mitnick RJ, Inglese M. A better characterization of spinal cord damage in multiple sclerosis: a diffusional kurtosis imaging study. American Journal of Neuroradiology. 2013;34(9):1846-52.

38.   Badawi AM DA, Youssef AM. Fuzzy logic algorithm for quantitative tissue characterization of diffuse liver diseases from ultrasound images. International Journal of Medical Informatics. 1999;55(2):135-47.

39.   Kadah YM FA, Zurada JM, Badawi AM. Classification algorithms for quantitative tissue characterization of diffuse liver disease from ultrasound images. Medical Imaging IEEE Transactions. 1996;15(4):466-78.

40.   Prakash KN RA, Suresh S, Chow TW. Fetal lung maturity analysis using ultrasound image features. IEEE Transactions Information Technology in Biomedicine. 2002;6(2):38-45.

41.   Guerriero S PM, Alcazar JL, Sedda F, Ajossa S, Mais V, Melis GB, Saba L. Tissue characterization using mean gray value analysis in deep infiltrating endometriosis. Ultrasound in Obstetrics and Gynecology. 2013;41:459-64.

42.   Marini C, Picano E, Varga A, Marzullo P, Pingitore A, Paterni M. Cyclic variation in myocardial gray level as a marker of viability in man. A videodensitometric study. European heart journal. 1996;17(3):472-9. Epub 1996/03/01.

43.   Aghini-Lombardi F, Di Bello V, Talini E, Di Cori A, Monzani F, Antonangeli L, et al. Early textural and functional alterations of left ventricular myocardium in mild hypothyroidism. Eur J Endocrinol. 2006;155(1):3-9. Epub 2006/06/24.

44.   Di Bello V, Monzani F, Giorgi D, Bertini A, Caraccio N, Valenti G, et al. Ultrasonic myocardial textural analysis in subclinical hypothyroidism. J Am Soc Echocardiogr. 2000;13(9):832-40. Epub 2000/09/09.

45.   Baroldi G, Bigi R, Cortigiani L. Ultrasound imaging versus morphopathology in cardiovascular diseases: the heart failure. Cardiovasc Ultrasound. 2007;5:5. Epub 2007/02/01.

46.   Aghini-Lombardi F, Di Bello V, Talini E, Di Cori A, Monzani F, Antonangeli L, et al. Early textural and functional alterations of left ventricular myocardium in mild hypothyroidism. European Journal of Endocrinology. 2006;155(1):3-9.

47.   Holland MR, Gibson AA, Peterson LR, Areces M, Schaffer JE, Perez JE, et al. Measurements of the cyclic variation of myocardial backscatter from two-dimensional echocardiographic images as an approach for characterizing diabetic cardiomyopathy. Journal of Cardiometabolic Syndrome. 2006;1(2):149-52.

48.   Voon WC, Chiu CC, Su HM, Chen HM, Hsieh CC, Huang JW, et al. Is pericardium a suitable calibration reference in integrated backscatter analysis? Ultrasound in Medicine and Biology. 2004;30(8):1063-6.

49.   Mizuno R, Fujimoto S, Saito Y, Nakamura S. Non-invasive quantitation of myocardial fibrosis using combined tissue harmonic imaging and integrated backscatter analysis in dilated cardiomyopathy. Cardiology. 2007;108(1):11-7. Epub 2006/09/09.

50.   Mohr GA, Vered Z, Barzilai B, Perez JE, Sobel BE, Miller JG. Automated determination of the magnitude and time delay ("phase") of the cardiac cycle dependent variation of myocardial ultrasonic integrated backscatter. Ultrason Imaging. 1989;11(4):245-59. Epub 1989/10/01.

51.   Finch-Johnston AE, Gussak HM, Mobley J, Holland MR, Petrovic O, Perez JE, et al. Cyclic variation of integrated backscatter: dependence of time delay on the echocardiographic view used and the myocardial segment analyzed. J Am Soc Echocardiogr. 2000;13(1):9-17. Epub 2000/01/08.

52.   Hiremath P, Bauer M, Cheng HW, Unno K, Liao R, Cheng S. Ultrasonic assessment of myocardial microstructure. Journal of Visualized Experiments. 2014(83):e50850.

53.   Teichholz LE, Kreulen T, Herman MV, Gorlin R. Problems in echocardiographic volume determinations: echocardiographic-angiographic correlations in the presence of absence of asynergy. The American journal of cardiology. 1976;37(1):7-11. Epub 1976/01/01.

54.   Bauer M, Cheng S, Unno K, Lin FC, Liao R. Regional cardiac dysfunction and dyssynchrony in a murine model of afterload stress. PloS one. 2013;8(4):e59915. Epub 2013/04/06.

55.   Bauer M, Cheng S, Jain M, Ngoy S, Theodoropoulos C, Trujillo A, et al. Echocardiographic speckle-tracking based strain imaging for rapid cardiovascular phenotyping in mice. Circulation research. 2011;108(8):908-16. Epub 2011/03/05.

56.   Hadi AM MK, Schalij I, Grunberg K, Meijer GA, Vonk-Noordegraaf A, van der Laarse WJ, Beliën JA. Rapid quantification of myocardial fibrosis: A new macro-based automated analysis. Analytical Cellular Pathology. 2010;33(5):257-69.

57.   Lang RM, Bierig M, Devereux RB, Flachskampf FA, Foster E, Pellikka PA, et al. Recommendations for chamber quantification: a report from the American Society of Echocardiography's Guidelines and Standards Committee and the Chamber Quantification Writing Group, developed in conjunction with the European Association of Echocardiography, a branch of the European Society of Cardiology. J Am Soc Echocardiogr. 2005;18(12):1440-63. Epub 2005/12/27.

58.   Franklin SS, Gustin Wt, Wong ND, Larson MG, Weber MA, Kannel WB, et al. Hemodynamic patterns of age-related changes in blood pressure. The Framingham Heart Study. Circulation. 1997;96(1):308-15. Epub 1997/07/01.

59.   Drazner MH. The progression of hypertensive heart disease. Circulation. 2011;123(3):327-34. Epub 2011/01/26.

60.   Urbano-Moral JA RE, Maron MS, Crean A, Pandian NG. Investigation of global and regional myocardial mechanics with 3-dimensional speckle tracking echocardiography and relations to hypertrophy and fibrosis in hypertrophic cardiomyopathy. Circulation Cardiovascular Imaging. 2014;7(1):11-9.

61.   Ciulla M, Paliotti R, Hess DB, Tjahja E, Campbell SE, Magrini F, et al. Echocardiographic patterns of myocardial fibrosis in hypertensive patients: endomyocardial biopsy versus ultrasonic tissue characterization. Journal of American Society of Echocardiography. 1997;10(6):657-64.

62.   Kovacs A, Courtois MR, Weinheimer CJ, Posdamer SH, Wallace KD, Holland MR, et al. Ultrasonic tissue characterization of the mouse myocardium: successful in vivo cyclic variation measurements. Journal of American Society of Echocardiography. 2004;17(8):883-92.

63.   Stuhlmuller JE, Skorton DJ, Burns TL, Melton HE, Jr., Vandenberg BF. Reproducibility of quantitative backscatter echocardiographic imaging in normal subjects. American Journal of Cardiology. 1992;69(5):542-6.

64.   Ito T IK, Dura I, Katagiri C, Maeda K. Tissue characterization of uterine myometrium using the ultrasound gray-level histogram width. Journal of Medical Ultrasonics. 2007;34:189-92.

65.   Ciulla M, Paliotti R, Hess DB, Tjahja E, Campbell SE, Magrini F, et al. Echocardiographic patterns of myocardial fibrosis in hypertensive patients: endomyocardial biopsy versus ultrasonic tissue characterization. J Am Soc Echocardiogr. 1997;10(6):657-64. Epub 1997/07/01.

66.   Bouki KP, Lange A, Palka P, Moran CM, Fenn LN, Wright RA, et al. Regional variations of ultrasonic integrated backscatter in normal and myopathic left ventricles. A new multi-view approach. European Heart Journal. 1996;17(11):1747-55.

67.   Di Bello V, Monzani F, Giorgi D, Bertini A, Caraccio N, Valenti G, et al. Ultrasonic myocardial textural analysis in subclinical hypothyroidism. Journal of American Society of Echocardiography. 2000;13(9):832-40.

68.   Di Bello V, Talarico L, Picano E, Di Muro C, Landini L, Paterni M, et al. Increased echodensity of myocardial wall in the diabetic heart: an ultrasound tissue characterization study. Journal of American College of Cardiology. 1995;25(6):1408-15.

69.   Holland MR, Gibson AA, Kirschner CA, Hicks D, Ludomirsky A, Singh GK. Intrinsic myoarchitectural differences between the left and right ventricles of fetal human hearts: an ultrasonic backscatter feasibility study. Journal of American Society of Echocardiography. 2009;22(2):170-6.

70.   Naito J, Masuyama T, Mano T, Kondo H, Yamamoto K, Nagano R, et al. Ultrasonic myocardial tissue characterization in patients with dilated cardiomyopathy: value in noninvasive assessment of myocardial fibrosis. American Heart Journal. 1996;131(1):115-21.

71.   Salvetti M, Muiesan ML, Paini A, Monteduro C, Bonzi B, Galbassini G, et al. Myocardial ultrasound tissue characterization in patients with chronic renal failure. Journal of American Society of Nephrology. 2007;18(6):1953-8.

72.   Feinberg MS, Gussak HM, Davila-Roman VG, Baumann CM, Miller JG, Perez JE. Dissociation between wall thickening of normal myocardium and cyclic variation of backscatter during inotropic stimulation. Am J Cardiol. 1996;77(7):515-20. Epub 1996/03/01.

73.   Fuentes VL, Moran CM, Schober K, McEwan JD, Brown H, Sutherland GR, et al. Measurement of cyclic variation in ultrasonic integrated backscatter in conscious, unsedated, clinically normal dogs. American Journal of Veterinary Research. 1997;58(10):1055-9.

74.   Hancock JE, Cooke JC, Monaghan MJ. Effect of harmonic imaging on the measurement of ultrasonic integrated backscatter and its interpretation in patients following myocardial infarction. European Journal of Echocardiography. 2004;5(3):189-95.

75.   Hunt KJ, Evans GW, Folsom AR, Sharrett AR, Chambless LE, Tegeler CH, et al. Acoustic shadowing on B-mode ultrasound of the carotid artery predicts ischemic stroke: the Atherosclerosis Risk in Communities (ARIC) study. Stroke. 2001;32(5):1120-6. Epub 2001/09/06.

76.   Picano E, Pelosi G, Marzilli M, Lattanzi F, Benassi A, Landini L, et al. In vivo quantitative ultrasonic evaluation of myocardial fibrosis in humans. Circulation. 1990;81(1):58-64.

77.   Wolverson MK BH, Peterson GJ. Ultrasonic tissue characterization of atheromatous plaques using a high resolution real time scanner. Ultrasound in Medicine and Biology. 1983;9(6):599-609.

78.   Bertini M, Delgado V, den Uijl DW, Nucifora G, Ng AC, van Bommel RJ, et al. Prediction of cardiac resynchronization therapy response: value of calibrated integrated backscatter imaging. Circulation: Cardiovascular Imaging. 2010;3(1):86-93.

79.   D'Hooge J, Heimdal A, Jamal F, Kukulski T, Bijnens B, Rademakers F, et al. Regional strain and strain rate measurements by cardiac ultrasound: principles, implementation and limitations. European Journal of Echocardiography. 2000;1(3):154-70.

80.   Roosens B, Droogmans S, Hostens J, Somja J, Delvenne E, Hernot S, et al. Integrated backscatter for the in vivo quantification of supraphysiological vitamin D(3)-induced cardiovascular calcifications in rats. Cardiovascular Toxicology. 2011;11(3):244-52.

81.   Hunt KJ, Sharrett AR, Chambless LE, Folsom AR, Evans GW, Heiss G. Acoustic shadowing on B-mode ultrasound of the carotid artery predicts CHD. Ultrasound Med Biol. 2001;27(3):357-65. Epub 2001/05/23.

82.   Olshansky B, Collins SM, Skorton DJ, Prasad NV. Variation of left ventricular myocardial gray level on two-dimensional echocardiograms as a result of cardiac contraction. Circulation. 1984;70(6):972-7.

83.   Meunier J, Bertrand M. Echographic image mean gray level changes with tissue dynamics: a system-based model study. IEEE transactions on bio-medical engineering. 1995;42(4):403-10. Epub 1995/04/01.

84.   O'Brien PD, O'Brien WD, Jr., Rhyne TL, Warltier DC, Sagar KB. Relation of ultrasonic backscatter and acoustic propagation properties to myofibrillar length and myocardial thickness. Circulation. 1995;91(1):171-5.

85.   Kurtz TW, Griffin KA, Bidani AK, Davisson RL, Hall JE. Recommendations for blood pressure measurement in humans and experimental animals. Part 2: Blood pressure measurement in experimental animals: a statement for professionals from the subcommittee of professional and public education of the American Heart Association council on high blood pressure research. Hypertension. 2005;45(2):299-310. Epub 2004/12/22.

86.   Baldwin SL, Holland MR, Sosnovik DE, Miller JG. Effects of region-of-interest length on estimates of myocardial ultrasonic attenuation and backscatter. Medical physics. 2005;32(2):418-26. Epub 2005/03/26.

87.   Barzilai B, Thomas LJ, 3rd, Glueck RM, Saffitz JE, Vered Z, Sobel BE, et al. Detection of remote myocardial infarction with quantitative real-time ultrasonic characterization. J Am Soc Echocardiogr. 1988;1(3):179-86. Epub 1988/05/01.

88.   Lin SL, Liu RH, Leu FJ, Shih JM, I MK, Kuo JS, et al. Detection of acute myocardial infarction by evaluation of ultrasonic gray levels in dogs. Jpn Heart J. 1991;32(5):687-99. Epub 1991/09/01.

89.   Mimbs JW, O'Donnell M, Miller JG, Sobel BE. Detection of cardiomyopathic changes induced by doxorubicin based on quantitative analysis of ultrasonic backscatter. Am J Cardiol. 1981;47(5):1056-60. Epub 1981/05/01.

90.   Fuentes VL, Moran CM, Schober K, McEwan JD, Brown H, Sutherland GR, et al. Measurement of cyclic variation in ultrasonic integrated backscatter in conscious, unsedated, clinically normal dogs. Am J Vet Res. 1997;58(10):1055-9. Epub 1997/11/05.

91.   Kovacs A, Courtois MR, Weinheimer CJ, Posdamer SH, Wallace KD, Holland MR, et al. Ultrasonic tissue characterization of the mouse myocardium: successful in vivo cyclic variation measurements. J Am Soc Echocardiogr. 2004;17(8):883-92. Epub 2004/07/30.

92.   Milunski MR, Mohr GA, Wear KA, Sobel BE, Miller JG, Wickline SA. Early identification with ultrasonic integrated backscatter of viable but stunned myocardium in dogs. Journal of the American College of Cardiology. 1989;14(2):462-71. Epub 1989/08/01.

93.   D'Hooge J, Heimdal A, Jamal F, Kukulski T, Bijnens B, Rademakers F, et al. Regional strain and strain rate measurements by cardiac ultrasound: principles, implementation and limitations. European journal of echocardiography : the journal of the Working Group on Echocardiography of the European Society of Cardiology. 2000;1(3):154-70. Epub 2002/03/28.

94.   Kubota T, Kawasaki M, Takasugi N, Takeyama U, Ishihara Y, Okubo M, et al. Evaluation of left atrial degeneration for the prediction of atrial fibrillation: usefulness of integrated backscatter transesophageal echocardiography. JACC Cardiovascular imaging. 2009;2(9):1039-47. Epub 2009/09/19.

95.   Pacileo G, Calabro P, Limongelli G, Russo MG, Pisacane C, Sarubbi B, et al. Left ventricular remodeling, mechanics, and tissue characterization in congenital aortic stenosis. J Am Soc Echocardiogr. 2003;16(3):214-20. Epub 2003/03/06.

96.   Angermann CE, Nassau K, Stempfle HU, Kruger TM, Drewello R, Junge R, et al. Recognition of acute cardiac allograft rejection from serial integrated backscatter analyses in human orthotopic heart transplant recipients. Comparison with conventional echocardiography. Circulation. 1997;95(1):140-50. Epub 1997/01/07.

97.   Suwa M, Ito T, Nakamura T, Miyazaki S. Prognostic implications derived from ultrasonic tissue characterization with myocardial integrated backscatter in patients with dilated cardiomyopathy. International journal of cardiology. 2002;84(2-3):133-40. Epub 2002/07/20.

98.   Hancock JE, Cooke JC, Monaghan MJ. Effect of harmonic imaging on the measurement of ultrasonic integrated backscatter and its interpretation in patients following myocardial infarction. European journal of echocardiography : the journal of the Working Group on Echocardiography of the European Society of Cardiology. 2004;5(3):189-95. Epub 2004/05/19.

99.   Salvetti M, Muiesan ML, Paini A, Monteduro C, Bonzi B, Galbassini G, et al. Myocardial ultrasound tissue characterization in patients with chronic renal failure. Journal of the American Society of Nephrology : JASN. 2007;18(6):1953-8. Epub 2007/04/20.

100.   Di Bello V, Talarico L, Picano E, Di Muro C, Landini L, Paterni M, et al. Increased echodensity of myocardial wall in the diabetic heart: an ultrasound tissue characterization study. Journal of the American College of Cardiology. 1995;25(6):1408-15. Epub 1995/05/01.

101.   Holland MR, Gibson AA, Peterson LR, Areces M, Schaffer JE, Perez JE, et al. Measurements of the cyclic variation of myocardial backscatter from two-dimensional echocardiographic images as an approach for characterizing diabetic cardiomyopathy. J Cardiometab Syndr. 2006;1(2):149-52. Epub 2007/08/19.

102.   Bertini M, Delgado V, den Uijl DW, Nucifora G, Ng AC, van Bommel RJ, et al. Prediction of cardiac resynchronization therapy response: value of calibrated integrated backscatter imaging. Circulation Cardiovascular imaging. 2010;3(1):86-93. Epub 2009/11/19.

103.   Lucarini AR TL, Di Bello V, Paterni M, Pedrinelli R, Picano E. Increased myocardial ultrasonic reflectivity is associated with extreme hypertensive left ventricular hypertrophy: a tissue characterization study in humans. American Journal of Hypertension. 1998;11(12):1442-9.

104.   Romano MM, Maciel LM, Almeida-Filho OC, Pazin-Filho A, Schmidt A, Maciel BC. Myocardial ultrasonic tissue characterization in patients with thyroid dysfunction. Cardiovascular ultrasound. 2010;8(8):15. Epub 2010/04/27.

105.   Stuhlmuller JE, Skorton DJ, Burns TL, Melton HE, Jr., Vandenberg BF. Reproducibility of quantitative backscatter echocardiographic imaging in normal subjects. Am J Cardiol. 1992;69(5):542-6. Epub 1992/02/25.

106.   Holland MR, Gibson AA, Kirschner CA, Hicks D, Ludomirsky A, Singh GK. Intrinsic myoarchitectural differences between the left and right ventricles of fetal human hearts: an ultrasonic backscatter feasibility study. J Am Soc Echocardiogr. 2009;22(2):170-6. Epub 2009/01/10.

107.   Koyama J, Ray-Sequin PA, Falk RH. Prognostic significance of ultrasound myocardial tissue characterization in patients with cardiac amyloidosis. Circulation. 2002;106(5):556-61.

108.   Vered Z, Mohr GA, Barzilai B, Gessler CJ, Jr., Wickline SA, Wear KA, et al. Ultrasound integrated backscatter tissue characterization of remote myocardial infarction in human subjects. Journal of the American College of Cardiology. 1989;13(1):84-91. Epub 1989/01/01.

109.   Milunski MR, Mohr GA, Perez JE, Vered Z, Wear KA, Gessler CJ, et al. Ultrasonic tissue characterization with integrated backscatter. Acute myocardial ischemia, reperfusion, and stunned myocardium in patients. Circulation. 1989;80(3):491-503. Epub 1989/09/01.

110.   Komuro K, Yamada S, Mikami T, Yoshinaga K, Noriyasu K, Goto K, et al. Sensitive detection of myocardial viability in chronic coronary artery disease by ultrasonic integrated backscatter analysis. J Am Soc Echocardiogr. 2005;18(1):26-31. Epub 2005/01/08.

111.   Bouki KP, Lange A, Palka P, Moran CM, Fenn LN, Wright RA, et al. Regional variations of ultrasonic integrated backscatter in normal and myopathic left ventricles. A new multi-view approach. European heart journal. 1996;17(11):1747-55. Epub 1996/11/01.

112.   Naito J, Masuyama T, Mano T, Kondo H, Yamamoto K, Nagano R, et al. Ultrasonic myocardial tissue characterization in patients with dilated cardiomyopathy: value in noninvasive assessment of myocardial fibrosis. American heart journal. 1996;131(1):115-21. Epub 1996/01/01.

113.   Hopkins WE, Waggoner AD, Gussak H. Quantitative ultrasonic tissue characterization of myocardium in cyanotic adults with an unrepaired congenital heart defect. Am J Cardiol. 1994;74(9):930-4. Epub 1994/11/01.

114.   Masuyama T, Valantine HA, Gibbons R, Schnittger I, Popp RL. Serial measurement of integrated ultrasonic backscatter in human cardiac allografts for the recognition of acute rejection. Circulation. 1990;81(3):829-39.

115.   Lee HH, Hung CS, Wu XM, Wu VC, Liu KL, Wang SM, et al. Myocardial ultrasound tissue characterization of patients with primary aldosteronism. Ultrasound Med Biol. 2013;39(1):54-61. Epub 2012/12/04.

116.   Di Bello V, Talini E, Delle Donne MG, Aghini-Lombardi F, Monzani F, La Carrubba S, et al. New echocardiographic techniques in the evaluation of left ventricular mechanics in subclinical thyroid dysfunction. Echocardiography. 2009;26(6):711-9.

Tables and Figures

Table 1. Prior Studies of Ultrasound Methods for Cardiac Microstructure Assessment

Method	No. Studies	Subjects per Study	Disease Phenotypes	Histologic Correlation	Outcomes Data
Animal Studies					
Integrated backscatter	4	7 to 25	Normal contractility,[86] coronary ligation,[87, 88] doxorubicin[89]	2 studies[87, 88]	--
Cyclic variation of integ. backscatter	5	1 to 11	Normal physiology,[84, 90, 91] coronary ischemia and reperfusion[87, 92]	1 study[87]	--
Human Studies					
Integrated backscatter and similar methods	17	1 to 159	Normal,[29, 93] AF,[94] aortic stenosis,[95] cardiac allografts,[96] cardiomyop.,[76, 97] CAD,[98] CKD,[99] IDDM,[100] DM2,[101] dyssynchrony,[42, 102] HTN,[65, 103] hypothyroid[44, 104]	4 studies [65, 76, 94, 96]	None
Cyclic variation of integrated backscatter	15	14 to 62	Normal,[105, 106] amyloidosis,[107] CAD,[108-110] cardiomyopathy,[111, 112] congenital heart dz,[113] cardiac allografts,[114] HTN,[31] dobutamine,[72] hyperaldosteronism,[115] hypothyroid[43, 116]	2 studies[112][112, 114]	None

Table 2. Validation of Reproducibility Characteristics

Variable	Treatment	Baseline variability (%)	Intra-user reproducibility (R^2)	Cyclical variability
ROI Structures	Regional ROI	41.6-48.8	------	High
	Full Myocardium	19.4-24.5	------	Low
ROI Size	Small	41.6-48.8	0.71-0.80	Unreliable
	Large	22.5-29.8	0.87-0.97	High
Use of Reference	Raw density	22.5-29.8	------	Unreliable
	Density ratio	27.8-33.9	------	Moderate

Table 3. Characteristics of the Clinical Study Sample

Characteristics	Healthy Controls (N=28)	Hypertensives (N=30)	P value
Clinical			
Age	52±9	54±3	0.24
Women, %	56	47	0.34
Systolic blood pressure, mmHg	121±9	142±19	<0.001
Diastolic blood pressure, mmHg	72±9	85±12	<0.001
Mean arterial pressure, mmHg	112±10	132±16	<0.001
Echocardiographic			
LV wall thickness, cm	1.8±0.2	1.9±0.3	0.33
LV end-diastolic diameter, cm	4.0±0.5	4.0±0.5	0.87
LV mass, g	146±56	149±44	0.84
Relative wall thickness	0.45±0.01	0.47±0.07	0.079
Fractional shortening	0.28±0.08	0.27±0.15	0.86
Ejection fraction, %	62±4	63±3	0.35
E prime, cm/s	13.2±3.1	10.1±2.8	0.0002
E/a ratio	1.2±4.2	1.1±4.0	0.36
E/e' ratio	6.2±1.6	7.5±2.1	0.014
Signal intensity coefficient	0.23±0.11	0.31±0.15	0.029

Values are shown as means±standard deviations or percent frequencies.

Table 4. Associations of Echocardiographic Parameters with Hypertension Status

	Hypertension Status	
	Est. Coeff (SE)*	**P value**
Unadjusted		
Left ventricular wall thickness, cm	0.066 (0.067)	0.33
Left ventricular end-diastolic diameter, cm	-0.011 (0.067)	0.87
Left ventricular mass, g	0.013 (0.067)	0.84
Relative wall thickness	0.117 (0.066)	0.079
E prime, cm/s	-0.236 (0.059)	0.0002
E/a ratio	-0.062 (0.067)	0.36
E/e' ratio	0.161 (0.064)	0.014
Signal intensity coefficient	0.144 (0.065)	0.029
Adjusted for age and sex		
Left ventricular wall thickness, cm	0.071 (0.078)	0.37
Left ventricular end-diastolic diameter, cm	-0.035 (0.079)	0.66
Left ventricular mass, g	-0.002 (0.081)	0.98
Relative wall thickness	0.118 (0.065)	0.076
E prime, cm/s	-0.272 (0.070)	0.0003
E/a ratio	-0.050 (0.068)	0.47
E/e' ratio	0.153 (0.071)	0.036
Signal intensity coefficient	0.153 (0.066)	0.025

*Estimated regression coefficients represent the change in blood pressure measure per 1-SD change in the echocardiographic parameter.

Table 5. Associations of Echocardiographic Parameters with Blood Pressure Indices

	Systolic Blood Pressure		Diastolic Blood Pressure		Mean Arterial Pressure	
	Est. Coeff (SE)*	P value	Est. Coeff (SE)*	P value	Est. Coeff (SE)*	P value
Unadjusted						
LVWT	2.73 (2.57)	0.29	3.83 (1.67)	0.025	4.74 (2.26)	0.041
LVDD	-0.23 (2.62)	0.93	0.90 (1.76)	0.61	0.83 (2.37)	0.73
LV mass	1.12 (2.63)	0.67	2.61 (1.74)	0.14	2.98 (2.36)	0.21
RWT	3.61 (2.44)	0.14	3.92 (1.59)	0.017	5.12 (2.14)	0.020
E prime	-5.75 (2.58)	0.030	0.56 (1.82)	0.76	-1.36 (2.44)	0.58
E/a ratio	-1.88 (2.54)	0.46	0.92 (1.72)	0.59	0.30 (2.32)	0.90
E/e' ratio	4.40 (2.43)	0.08	-0.54 (1.68)	0.75	0.93 (2.26)	0.68
SIC	5.45 (2.40)	0.027	4.05 (1.60)	0.014	5.87 (2.14)	0.008
Adjusted for age and sex						
LVWT	2.30 (2.80)	0.41	2.34 (1.85)	0.21	3.11 (2.52)	0.22
LVDD	-1.48 (2.87)	0.61	-1.49 (1.90)	0.44	-1.98 (2.59)	0.45
LV mass	0.03 (2.95)	0.99	0.55 (1.96)	0.78	0.55 (2.67)	0.84
RWT	3.69 (2.36)	0.12	3.85 (1.51)	0.014	3.80 (1.59)	0.021
E prime	-6.05 (2.89)	0.041	-1.44 (2.00)	0.48	-2.98 (2.06)	0.16
E/a ratio	-1.75 (2.53)	0.49	0.11 (1.69)	0.95	-0.51 (1.77)	0.78
E/e' ratio	3.94 (2.60)	0.14	0.72 (1.77)	0.69	1.79 (1.84)	0.33
SIC	4.79 (2.41)	0.053	3.34 (1.60)	0.042	3.83 (1.66)	0.026

LVWT, left ventricular wall thickness; LVDD, left ventricular end-diastolic diameter; RWT, relative wall thickness; SIC, signal intensity coefficient.
*Estimated regression coefficients represent the change in blood pressure measure per 1-SD change in the echocardiographic parameter.

Table 6. Clinical and Imaging Characteristics By Genotype-Phenotype Groups

Characteristic	Overt HCM (G+/LVH+)	P value*	Subclinical HCM (G+/LVH-)	P value†	Control (G-/LVH-)	P value‡
N	10		10		10	
Age, y	47.9 (17.7)	0.0006	37.0 (10.9)	0.09	25.9 (6.1)	0.007
Female, %	20 (42)	0.11	80 (42)	0.003	50 (53)	0.15
Conventional Echocardiographic Measures						
LV mass, g	179 (78)	0.003	83.7 (18.4)	0.0006	97.3 (28.6)	0.19
Maximum LV wall thickness	17.6 (6.1)	<0.0001	7.3 (1.3)	<0.0001	7.8 (1.8)	0.45
LV ejection fraction, %	58.1 (14.6)	0.72	64 (6)	0.19	60 (4)	0.04
Global E' velocity, cm/s	9.3 (1.9)	<0.0001	12.7 (1.7)	0.008	16.0 (2.1)	0.001
Microstructural Measures						
LGE, g	26.7 (34.6)	----	0 (0)	----	0 (0)	----
LGE, % LV mass	12.9 (12.6)	----	0 (0)	----	0 (0)	----
ECV (average)	0.393 (0.044)	<0.0001	0.336 (0.042)	0.005	0.254 (0.023)	<0.0001
ECV excluding LGE	0.390 (0.042)	<0.0001	0.336 (0.042)	0.006	0.254 (0.023)	<0.0001
Signal intensity coefficient	0.429 (0.046)	<0.0001	0.290 (0.055)	<0.0001	0.162 (0.053)	<0.0001
Serum Biomarker Levels						
PICP, ug/L	111 (22.6)	0.06	76.5 (17.1)	0.006	78.9 (32.3)	0.85
Singulex TnI, pg/mL	11.9 (7.64)	0.05	2.89 (1.74)	0.008	4.86 (4.77)	0.31
NT-proBNP, pg/mL	654 (1050)	0.11	41.5 (34.3)	0.12	28.5 (28.2)	0.44

Values are shown as mean ± standard error adjusted for age, sex, and family relation.

LV, left ventricular; LGE, late gadolinium enhancement; ECV, extracellular volume; PICP, carboxy-terminal propeptide of procollagen type I; TnI, cardiac troponin I; NT-proBNP, N-terminal of B-type natriuretic peptide.

*Comparison between overt HCM and control groups.

†Comparison between overt HCM and subclinical HCM groups.

‡Comparison between subclinical HCM and control groups

Table 7. Correlations of Clinical, Echocardiographic, MRI, and Biomarker measures in the HCM cohort

	Age	Female (fraction)	PICP	Singulex TnI	NT-proBNP	LV mass	Maximum LV wall thickness	LVEF	Global E'	LGE	ECV
Age											
Female (fraction)	0.49										
PICP	-0.17	-0.63									
Singulex TnI	-0.10	-0.54	0.63								
NT-proBNP	-0.21	-0.27	0.43	0.72							
LV mass	0.26	-0.64	0.52	0.85	0.65						
Max LV wall thickness	0.43	-0.46	0.42	0.22	-0.12	0.61					
LVEF	-0.14	0.27	0.12	-0.14	0.01	-0.24	-0.24				
Global E' velocity	-0.61	0.09	-0.83	-0.19	-0.74	-0.49	-0.72	0.10			
LGE	-0.79	-0.39	*	*	*	0.43	-0.69	0.19	0.44		
ECV (average)	0.57	-0.09	0.19	0.44	0.64	0.41	0.38	0.18	-0.71	0.75	
SIC	0.57	-0.20	0.34	0.50	0.50	0.56	0.61	0.05	-0.84	0.38	0.85

Values are shown as Pearson correlation coefficients.

LV, left ventricular; LGE, late gadolinium enhancement; ECV, extracellular volume; PICP, carboxy-terminal propeptide of procollagen type I; TnI, cardiac troponin I; NT-proBNP, N-terminal of B-type natriuretic peptide. SIC, signal intensity coefficient.

*Analyses omitted due to insufficient sample size

Figure 1. Roles of conventional ultrasound and microstructural ultrasound-based imaging in assessment of cardiac remodeling. Conventional ultrasound is used to assess different macrostructural phenotypes of hypertrophy (Panel A). Changes in relative wall thickness (RWT) and left ventricular mass (LV mass) may be quantified and may be measured using an image such as this parasternal long axis B-mode echocardiographic image (Panel B). Histologic analyses can be performed to identify cardiac remodeling changes in the microstructure, or tissue, including fibrosis and cellular dysfunction. On ultrasound, a region of interest shows grayscale pixels that are influenced by microstructural changes including fibrosis and cellular dysfunction. Therefore, ultrasound may serve to identify microstructural changes in parallel with histology.
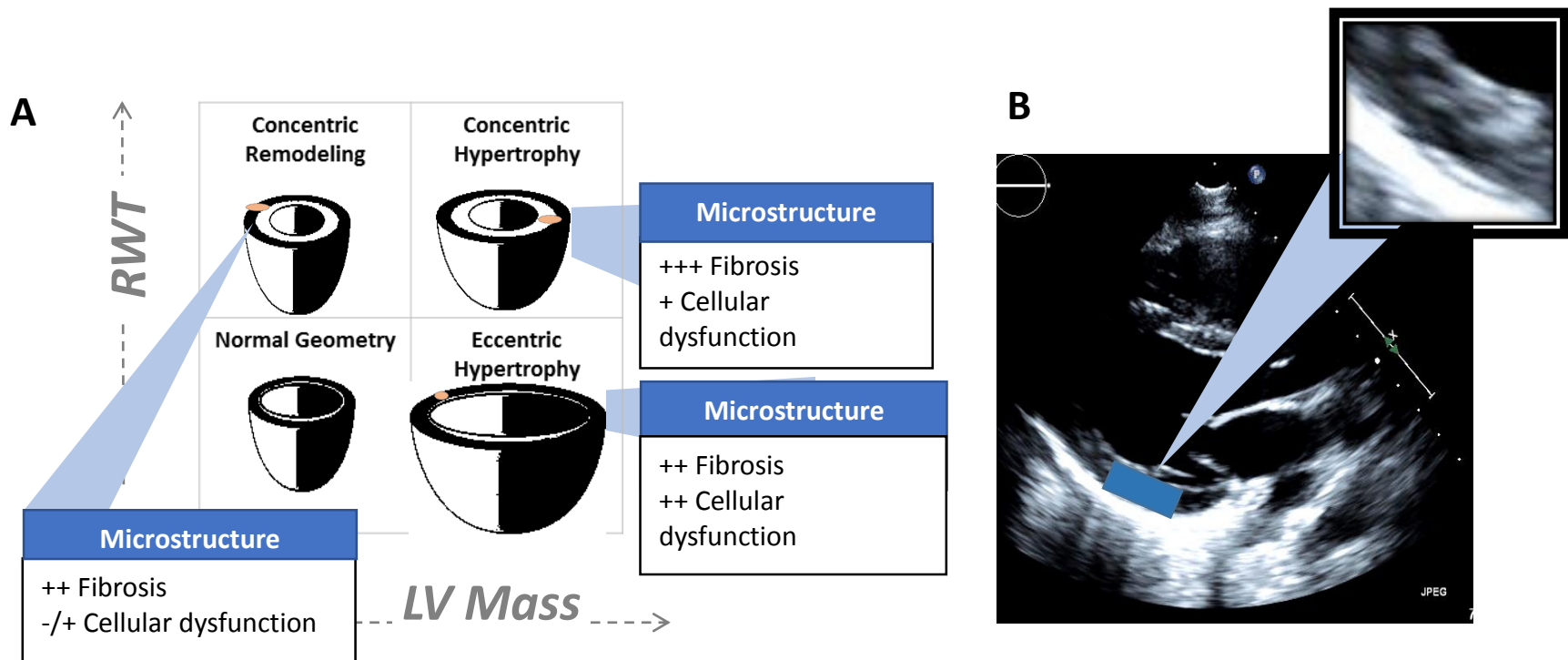
Figure 2. Workflow process for algorithm application. Four main steps may be repeated in any analysis, including subject comparison and quantification of cyclical variability.
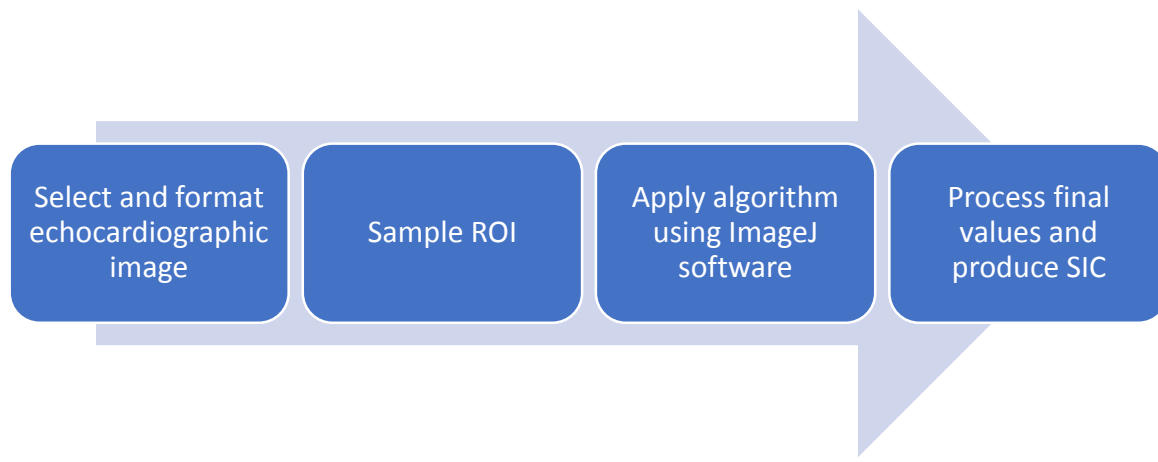
Figure 3. Creation of a signal distribution. Within the grayscale image, a region of interest may be selected, such as the orange box within the myocardium (panel A). The ImageJ algorithm assigns each pixel a grayscale intensity value between 0 and 255, as is seen in the representative grid (panel B). A frequency histogram can be created after hierarchically re-arranging the grayscale intensities, and this curve is termed the signal distribution (panel C).
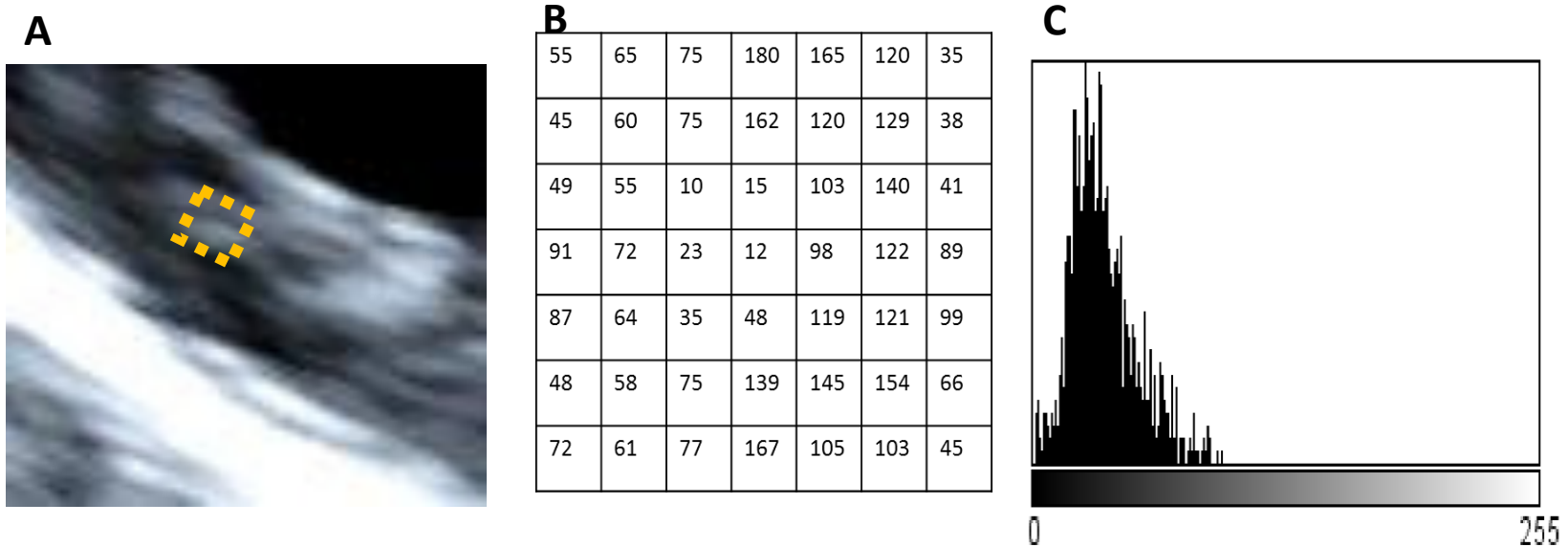
A

B

55	65	75	180	165	120	35
45	60	75	162	120	129	38
49	55	10	15	103	140	41
91	72	23	12	98	122	89
87	64	35	48	119	121	99
48	58	75	139	145	154	66
72	61	77	167	105	103	45

C

0   255

Figure 4. Signal distribution analysis and algorithm development. Standardized myocardial and pericardial selections for representative mouse (row A) and human end-diastolic images (row B) are shown. Signal intensity distributions are shown from single-frame analyses of representative mouse and human images, for region of interest (ROI) including full-screen (column 1), pericardial (column 2), and myocardial areas (column 3). The distributions of signal intensity are right-shifted for brighter areas such as the pericardium, and are larger in range for more heterogeneous areas.
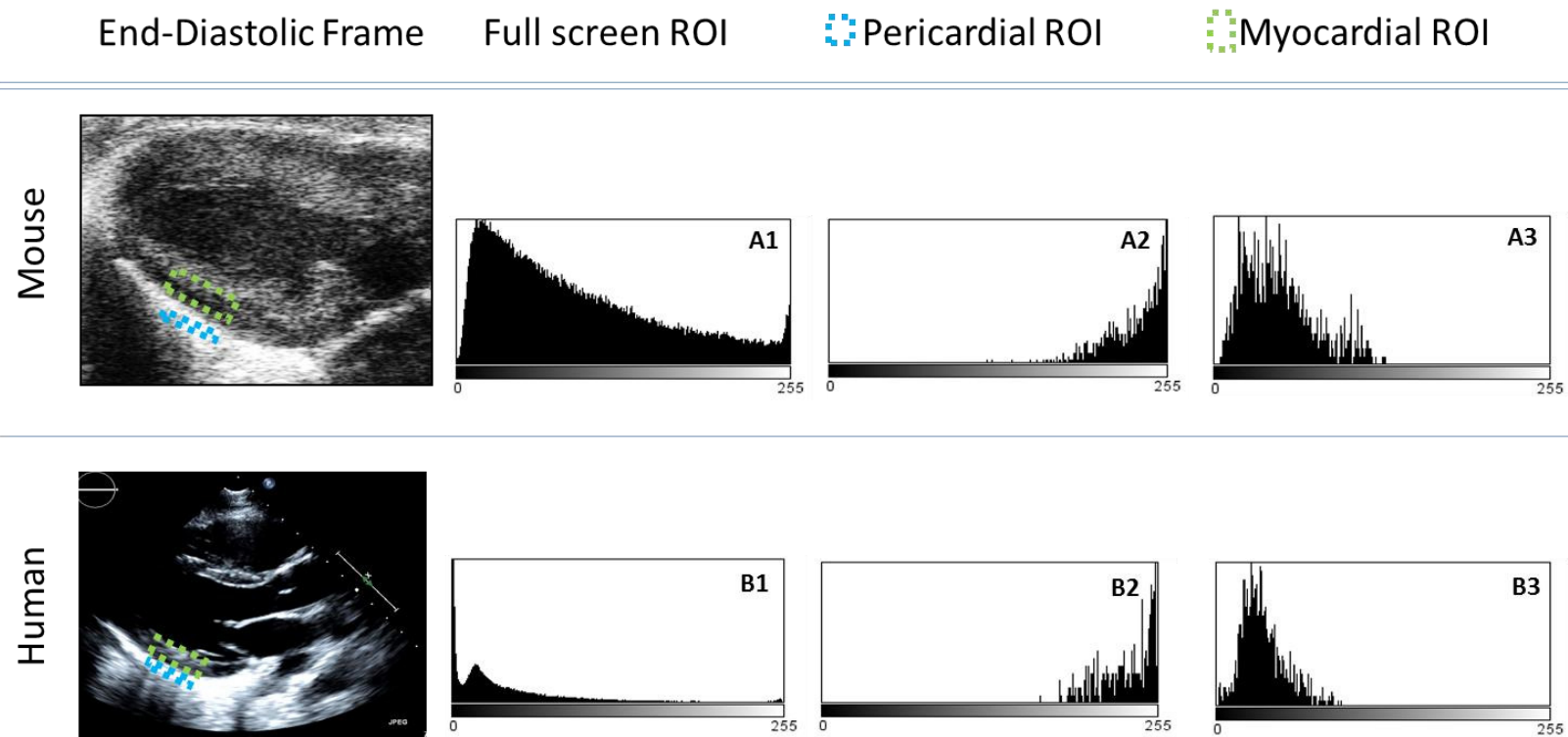
Figure 5. Variation of sonographic signal intensity during the cardiac cycle. Signal distributions were generated via the ImageJ algorithm for a myocardial ROI, over consecutive frames of an echocardiographic image. The analyses were performed for an aortic banded mouse (Panel A) and a representative control mouse (Panel B). Frame rate was 212 for both images. Three markers were used to assess cyclical variability: 20th percentile (diamond), 50th percentile (square), and 80th percentile (triangle). Relative cyclical variability was higher for the 80th percentile values than for the 20th and 50th percentile values. The myocardial grayscale signal intensity is lowest in end-diastolic frame, represented by the asterisk and vertical line.
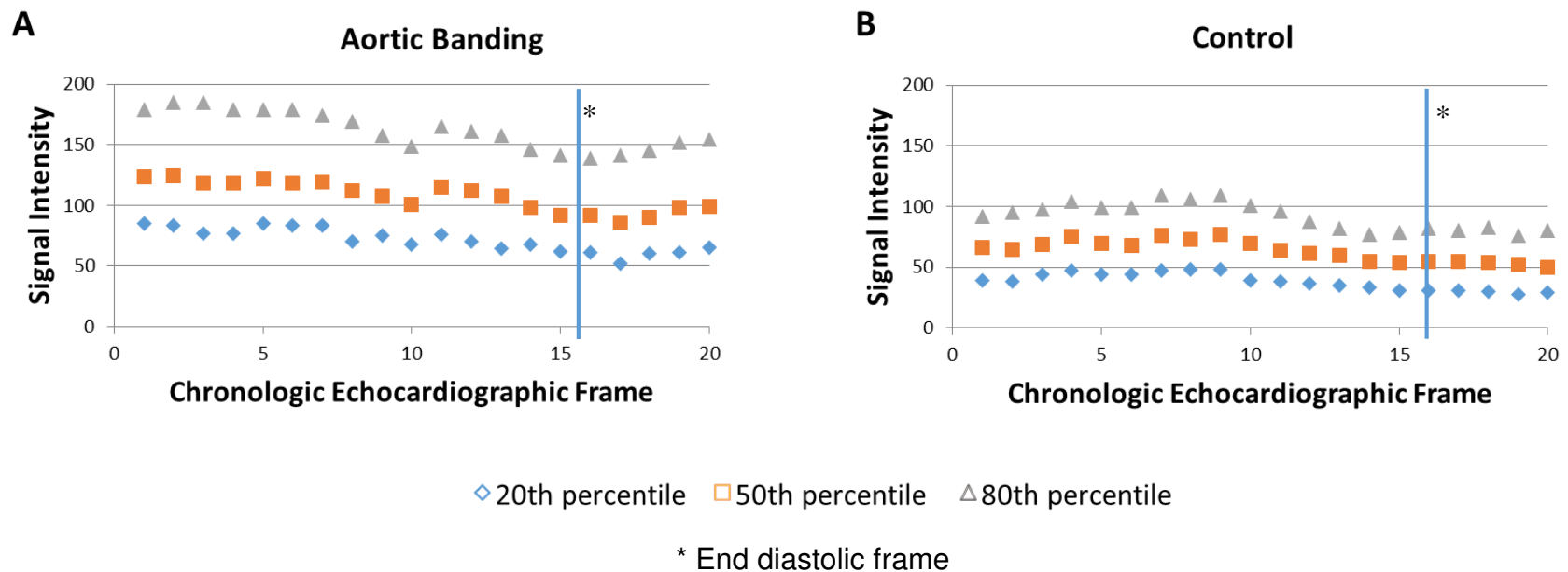
Figure 6. Variable afterload stress in mice. Mean (± standard error) values of conventional and advanced echocardiographic measures are displayed for each group of mice: vehicle control, banded and then debanded mice, and continually banded mice. Conventional echocardiographic measures include left ventricular mass (Panel A) and relative wall thickness (Panel B). Advanced measure represented as the signal intensity coefficient (Panel C). P values are for Kruskal-Wallis tests of difference between independent groups.
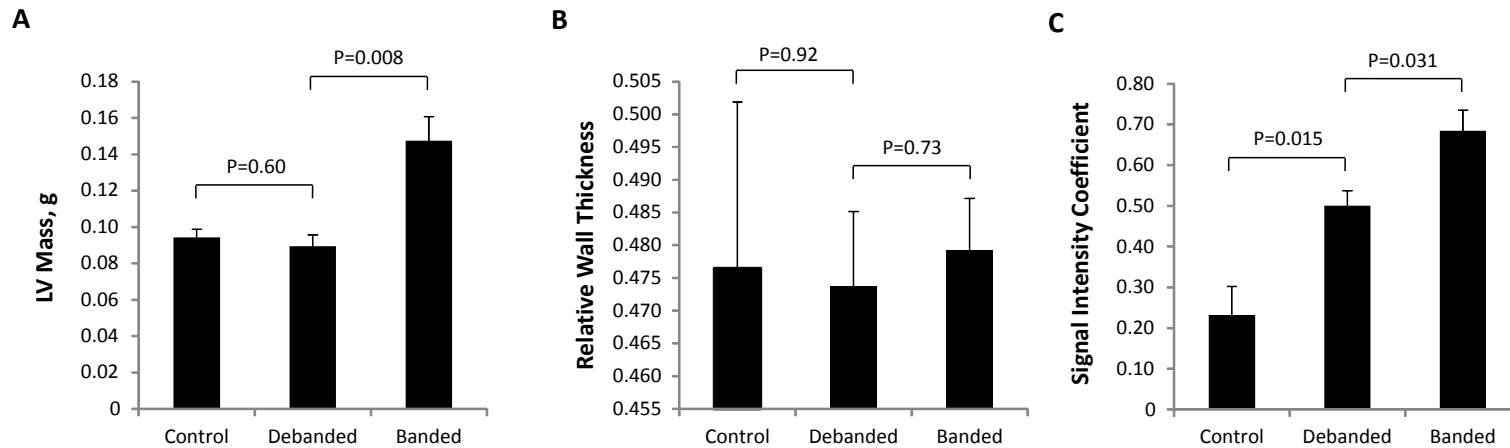
Figure 7. Histologic examination. Masson's trichrome stains of myocardial tissue are shown for representative mice from each of three animal groups: control (Panel A), debanded (Panel B), and banded (Panel C). The black horizontal scale bars demonstrate 50 micrometers.
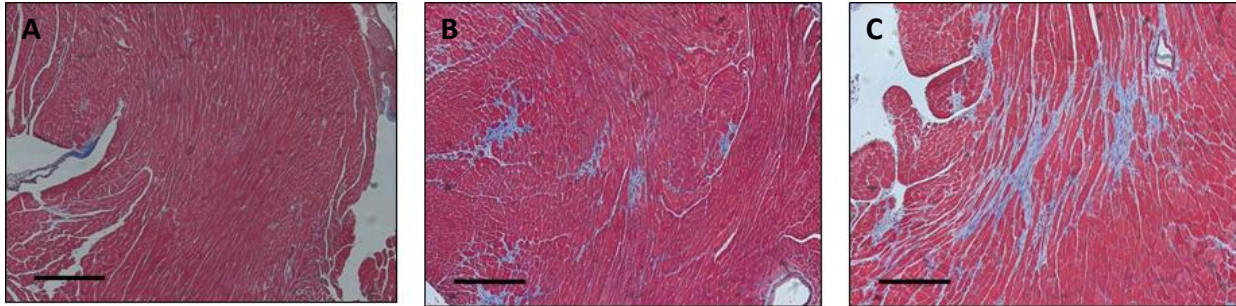
Figure 8. Mean (± standard error) values of conventional and advanced echocardiographic measures are displayed across increasing tertile of systolic (Panel A), diastolic (Panel B), and mean arterial (Panel C) pressure in the total study sample. Conventional echocardiographic measures include left ventricular mass and relative wall thickness; advanced measures include the signal intensity coefficient. P values are for non-parametric tests of trend across tertiles of each blood pressure measure.
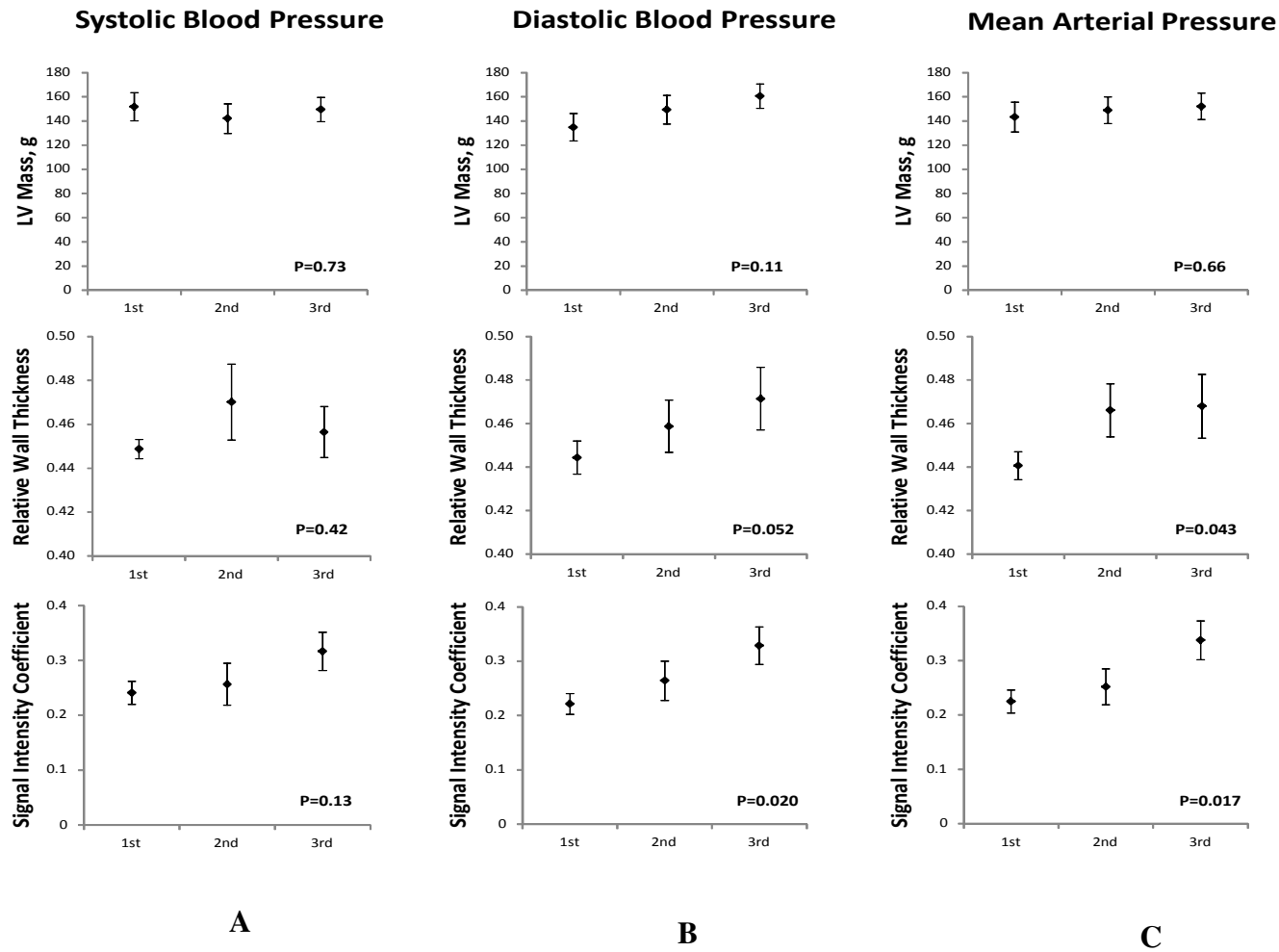
Figure 9. Mean (± standard error) values of left ventricular mass (Panel A), global E' velocity (Panel B), MRI measurement of extracellular volume (Panel C), and the sonographic measurement of signal intensity coefficient (Panel D) are displayed for overt HCM individuals (G+/LVH+), subclinical HCM individuals (G+/LVH-), and healthy controls (G-/LVH-). P values are for Kruskal-Wallis tests of difference between independent groups.